Atmospheric Environment 230 (2020) 117548

Contents lists available at ScienceDirect

Atmospheric Environment

journal homepage: http://www.elsevier.com/locate/atmosenv

Investigating multiple aerosol optical depth products from MODIS and VIIRS over Asia: Evaluation, comparison, and merging

Yuan Wang [a], Qiangqiang Yuan [a,e,f,*], Huanfeng Shen [b,d,f], Li Zheng [a], Liangpei Zhang [c,f]

[a] School of Geodesy and Geomatics, Wuhan University, Wuhan, Hubei, 430079, China
[b] School of Resource and Environmental Sciences, Wuhan University, Wuhan, Hubei, 430079, China
[c] The State Key Laboratory of Information Engineering in Surveying, Mapping and Remote Sensing, Wuhan University, Wuhan, Hubei, 430079, China
[d] The Key Laboratory of Geographic Information System, Ministry of Education, Wuhan University, Wuhan, Hubei, 430079, China
[e] The Key Laboratory of Geospace Environment and Geodesy, Ministry of Education, Wuhan University, Wuhan, Hubei, 430079, China
[f] The Collaborative Innovation Center for Geospatial Technology, Wuhan, Hubei, 430079, China

HIGHLIGHTS

- A total of four AOD products from MODIS and VIIRS were evaluated and compared against 80 AERONET sites in Asia.
- The evaluation and comparison results were analyzed considering aerosol loadings, time sequence, and AOD-related factors.
- A novel grid-based merging framework was proposed to absorb the strengths of the four AOD products from MODIS and VIIRS.
- The incorrect estimations for all AOD products in *forest* and for DB_M and DB_V in *arid lands* are mitigated after merging.

ARTICLE INFO

Keywords:
MODIS and VIIRS
AOD
Evaluation and comparison
Merging
Sub-grid weighting
Asia

ABSTRACT

The first purpose of this paper is to evaluate and compare four aerosol optical depth (AOD) products from the MODerate Resolution Imaging Spectroradiometer (MODIS) and the Visible Infrared Imaging Radiometer Suite (VIIRS) during 2013–2018 in Asia. In our study, a total of 81 AERONET sites are considered and land cover maps are utilized as well. The results show that the AOD product of deep blue from VIIRS (DB_V) achieves the best performance in the study areas, with the R of 0.91 and the RMSE of 0.14. Meanwhile, the deviations for the AOD products of deep blue from MODIS (DB_M), dark target (DT), DB_V, and environmental data record (EDR) periodically fluctuate with different levels as time moves forward. In general, DB_V overcomes others with the smallest overall deviation, while the largest positive and negative deviations are observed in DT and EDR, respectively. The performance of each AOD product is different in the regions with diverse land cover types. Especially, all AOD products will generally underestimate the AOD values in *forest*; DB_V performs better than DB_M in *croplands* and *urban*, while the overestimation of DB_V is larger than that of DB_M in *arid lands*. The distribution of high AOD values for DT and EDR shows difference in four seasons, which is dominated by multiple factors. With regard to DB_M and DB_V, apart from the seasonal variations, the high AOD values also distribute in *arid lands* from March to August. For the coverage of valid AOD values, the annual AOD completeness of DB_M and DB_V tends to be large in the Southwest (*arid lands*). As for DT and EDR, the large annual AOD completeness principally distributes in India, where the primary land cover type is *croplands*. Next, a novel grid-based merging framework (SL-SGW) is proposed to acquire the AOD product with the best performance and the largest AOD completeness of DB_M, DT, DB_V, and EDR as much as possible. The experiment results (2017–2018) show that the R and the RMSE for the merged AOD product are 0.904 and 0.13, respectively. It's believed that the merging framework could effectively absorb the strengths of DB_M, DT, DB_V, and EDR. In the meantime, the underestimations of the AOD values for all AOD products in *forest* and the overestimations for DB_M and DB_V in *arid lands* are both mitigated after merging. The AOD completeness of the merged exceeds those of other AOD products for all land cover types, particularly in *croplands* and *urban*.

* Corresponding author. School of Geodesy and Geomatics, Wuhan University, Wuhan, Hubei, 430079, China.
E-mail addresses: whuwy@yahoo.com (Y. Wang), yqiang86@gmail.com (Q. Yuan), shenhf@whu.edu.cn (H. Shen), lzheng@sgg.whu.edu.cn (L. Zheng), zlp62@whu.edu.cn (L. Zhang).

https://doi.org/10.1016/j.atmosenv.2020.117548
Received 10 January 2020; Received in revised form 12 April 2020; Accepted 20 April 2020
Available online 27 April 2020

1. Introduction

Aerosol includes tiny liquid and solid particles suspended in the air (Kaufman et al., 2002; Ramanathan et al., 2011), which affects the global climatic system directly and indirectly (Bingen et al., 2017; Cappucci and Gobron, 2017). Aerosol not only exerts direct effect through altering the radiation reaching the ground surface (Li et al., 2017b; Lohmann and Feichter, 2001; Yang et al., 2016) but also causes indirect effect by acting as cloud condensation nucleus, which mediately changes the cloud and precipitation (Guo et al., 2016, 2018; Twomey, 1977), even though it has an inconclusive effect on weather and climate systems (Fan et al., 2016; Rosenfeld et al., 2014; Li et al., 2019). Meanwhile, aerosol is considered as the main pollutant in the atmosphere, which has an influence on the air quality (Butt et al., 2017; Huang et al., 2014; Li et al., 2014). For instance, particulate matters (Guo et al., 2017a; Yang et al., 2019; Zou et al., 2019) at an aerodynamic equivalent diameter of less than 2.5 μm ($PM_{2.5}$) are capable of carrying and transporting toxic and noxious substances (Li et al., 2017a; Shen et al., 2018). Typically, one of the crucial parameters, i.e., aerosol optical depth (AOD), which is defined as the vertical integral of light extinction by aerosol in the atmospheric column, could describe aerosol optical properties (Della Ceca et al., 2018; Giles et al., 2012; Holben et al., 2001). Ground-based sites are commonly regarded as the most reliable and accurate approach to acquire AOD products (Giles et al., 2019; Holben et al., 1998), while they offer measurements at small center regions and fail to provide a global view of AOD distribution. Therefore, remote sensing satellites have been employed for retrieving AOD products to enlarge the AOD spatial coverage (Ahn et al., 2014; Kaufman et al., 2005; Kahn et al., 2010; Sayer et al., 2012; Zhang et al., 2019).

The MODerate Resolution Imaging Spectroradiometer (MODIS) is a passive remote sensing sensor onboard the Terra and Aqua satellites (Barnes et al., 1998), which is able to generate daily AOD products at both locally and globally distributed scales (Levy et al., 2013; Sayer et al., 2014). To be specific, the team of MODIS provides AOD products at 10-km spatial resolutions of the dark target (DT) algorithm (Levy et al., 2007, 2013; Gupta et al., 2016) and the MODIS deep blue (DB_M) algorithm (Hsu et al., 2004, 2013, 2019). Considering the fact that the Terra and Aqua satellites have served for more than ten years in excess of their design life, the Visible Infrared Imaging Radiometer Suite (VIIRS) sensor onboard the Suomi National Polar-Orbiting Partnership (Suomi NPP) satellite was launched in 2011 (Xiong et al., 2014), seen as the successor of MODIS. By contrast, VIIRS has a wider swath width of 3060 km, which avoids the scanning gaps of MODIS (2330 km) between two adjacent orbits in the low-latitude areas (Hsu et al., 2019; Sayer et al., 2015, 2019). Similarly, the team of VIIRS also provides AOD products at 6-km spatial resolution based on the environmental data record (EDR) algorithm (Jackson et al., 2013; Liu et al., 2014) and the VIIRS deep blue (DB_V) algorithm (Hsu et al., 2019; Sayer et al., 2019). Although the procedures of DB_V are similar to DB_M, several significant distinctions still exist in DB_V compared to DB_M, which result from the differences between MODIS and VIIRS, such as the spectral bands, aerosol models, sensor zenith angle ranges, and spatial resolutions.

The quality of AOD products is always a hot topic for the scientific community. In the past few years, numerous scholars have researched on the works related to the performance and spatiotemporal distribution (e.g., seasonal) of AOD products from MODIS and VIIRS. For example, Mhawish et al. (2017) validated the MODIS collection 6 (C6) AOD products over Indo-Gangetic plain and offered the abundant analyses of DT, DB_M, and DT&DB_M merged AOD products; Wang et al. (2019a) provided the detailed evaluation of the MODIS collection 6.1 (C6.1) AOD products over China and the assessed the improvements of AOD retrieval algorithms; Wei et al. (2017) compared MODIS C6 and VIIRS EDR AOD products in China and concluded that the DT and DB_M AOD products are more robust than EDR; Sayer et al. (2019) first evaluated the latest DB_M and DB_V AOD products at both global and regional scale and presented lots of valuable conclusions. However, there has not yet been a methodical evaluation of these latest DB products against other AOD products from MODIS and VIIRS, i.e., DT (C6.1) and EDR. Furthermore, the researches usually only indicated the strengths and defects of the AOD products rather than improved the quality of them after evaluation and comparison, which lack further significance for atmospheric science field. As is known to us, merging multiple AOD products could obtain the one with the best performance and the largest AOD completeness as much as possible. To date, lots of works have spared no effort to them, such as the Bayesian maximum entropy (BME) method (Tang et al., 2016), the customized methods (Bilal et al., 2017), and the spatial-temporal aerosol variation mitigation (ST-AVM) method (Wang et al., 2019b). As a result, it's a good choice to merge the AOD products from MODIS and VIIRS after evaluation and comparison to absorb the strengths of DB_M, DT, DB_V, and EDR, which is conducive to acquiring better AOD product from these two sensors.

The purpose of our study firstly aims at evaluating and comparing the latest AOD products from MODIS and VIIRS (DB_M, DT, DB_V, and EDR) during 2013–2018. Next, a novel grid-based merging framework, i.e., sub-grid weighting considering seasonality and land cover types (SL-SGW), is proposed to absorb the strengths of them, inspired by the methods of evaluation and comparison. Meanwhile, Asia is selected as the study areas in this paper for owning plenty of polluted regions and the diverse underlying surface, which is specifically illustrated in Section 2.1. The rest of our study is structured as follows. Section 2 introduces the study areas and datasets in our study. The evaluation and comparison results are given in Section 3, which are separated into the analyses according to three parts: aerosol loadings, temporal sequence, and AOD-related factors. Section 4 discusses the AOD spatiotemporal distribution and AOD completeness. The methodology and experiment results of SL-SGW are provided in Section 5. At last, Section 6 presents the conclusions.

2. Study areas and datasets

2.1. Study areas

In this paper, Asia with the largest population in seven continents is selected as the study areas (see Fig. 1). On the one hand, the aerosol properties of Asia are multiple and complex (Alam et al., 2014; Eck et al., 2005; Guo et al., 2017b), which is beneficial to the examinations of aerosol models hypotheses in the AOD retrieval algorithms. On the other hand, the land cover types of Asia are abundant as demonstrated in Fig. 2, which is favorable for the tests of surface reflectance estimations in the AOD retrieval algorithms. Meanwhile, Asia includes several typically polluted regions where plenty of works related to space-borne AOD evaluation have done in the past few years (Bilal et al., 2016; Che et al., 2018; Mhawish et al., 2017, 2019; Wei et al., 2019). In conclusion, it's reasonable to consider Asia as the study areas for the evaluation, comparison, and merging of the AOD products from MODIS and VIIRS. What is worth mentioning is that some regions in Fig. 1, which fall outside of Asia, are also considered in our study to obtain better analyses.

2.2. Datasets

In our study, the AOD products of DB_M, DT, DB_V, and EDR over land in Asia (1–78°N, 26–170°E) during 2013–2018 are employed. For DB_M and DT, since the overpass time of VIIRS is similar to the MODIS onboard Aqua instead of Terra, only the AOD products from Aqua-MODIS are considered. Meanwhile, the swaths of all AOD products are stitched and remapped to the geographical projection of World Geodetic System 1984) (WGS84) using the nearest neighbor interpolation (Parker et al., 1983) (0.1° × 0.1°for MODIS and 0.06° × 0.06°for VIIRS) in the range of study areas. In addition, the overlap regions are filled with the swath at the maximum overpass time. The ground-based measurements

(providing ground truth-values of AOD) and land cover maps (providing land cover types) are utilized as well to acquire a comprehensive study.

2.2.1. AEROsol robotic NETwork (AERONET)

The AERONET is a collection of ground-based Cimel Electronique Sun–sky radiometers, which has provided global measurements of aerosol products in the spectral range from 0.34 μm to 1.06 μm for more than two decades (Holben et al., 1998, 2001). At present, the AERONET database of Version 3 (Giles et al., 2019) includes separate three levels for data quality: Level 1.0 (prescreened), Level 1.5 (cloud-cleared and instrument-anomaly-controlled), and Level 2.0 (cloud-cleared, instrument-anomaly-controlled, and quality-assured). All of them could be obtained at the AERONET official website (https://aeronet.gsfc.nasa.gov). Due to the high accuracy and low uncertainty, the AOD measurements (Level 1.5 and Level 2.0, Version 3.0) of AERONET are regarded as the ground truth-values to evaluate the AOD products of DB_M, DT, DB_V, and EDR in our study. In addition, the measurements related to the spectral gradient of AOD across the wavelength range of 440–870 nm ($AE_{440\text{-}870}$) are also acquired from the AERONET database for further analyses. The distribution of AERONET sites over land in Asia is demonstrated in Fig. 2, with the marks of rectangles. Similarly, the AERONET sites distributed in the study areas (1–78°N, 26–170°E) but not in Asia are utilized as well. Hence, a total of 80 AERONET sites (see Table s1 in the supplementary materials) are used in our study, which contain various aerosol properties and land cover types.

2.2.2. The AOD products from MODIS and VIIRS

2.2.2.1. The MODIS DT AOD product. In summary, the DT algorithm in C6 makes use of the short-wave infrared (SWIR, 2.13 μm) band slightly influenced by the aerosol to recognize the regions over dark surface (low surface reflectance), following the procedure of screening (cloud and snow/ice). As per the surface modeling, the surface reflectance at 0.47, 0.65, and 1.24 μm is calculated in the DT algorithm. The top-of-atmosphere (TOA) reflectance at the 0.47 and 0.65 μm is then acquired to retrieve the AOD values at 0.55 μm using the look-up table (LUT), consisting of the aerosol models for coarse and fine particles (Levy et al., 2007). All the steps are employed with the single windows of 20 × 20 pixels at a 500-m spatial resolution. In the latest C6.1, considering the urban percentage as one part of the surface reflectance calculation, the DT algorithm modified the surface reflectance estimations on condition that the urban percentage exceeds 20% (Gupta et al., 2016). In our study, the record of DT in C6.1 with the highest quality assurance (QA = 3) over land is selected.

2.2.2.2. The MODIS and VIIRS DB AOD products. For MODIS, the DB_M algorithm initially was devised to retrieve aerosol properties over arid lands and urban areas, where the surface reflectance of the red and near-infrared bands usually shows a high degree. Nevertheless, the surface reflectance in these regions is greatly darker at the deep blue band (Hsu et al., 2004). Unlike the DT algorithm, DB_M firstly acquires AOD retrievals at a 1-km spatial resolution with the predetermined surface reflectance database and then aggregates them to a 10-km spatial resolution. After ten years, an enhanced algorithm that employs the combination of the precalculated database and the normalized difference vegetation index (NDVI) to obtain the surface reflectance has been developed (Hsu et al., 2013). As a consequence, the completeness of the AOD coverage has been extended to all land areas except snow/ice. In the latest C6.1, DB_M has been improved once more with some major updates, e.g., the modified surface modeling in elevated terrains and the heavy smoke detection (Hsu et al., 2019). As for VIIRS, the procedures of DB_V are similar with DB_M in C6.1, while some great distinctions still exist due to the differences of the spectral bands, the swath width, the sensor zenith angle range, and the spatial resolution between MODIS and VIIRS (Hsu et al., 2019). For instance, a modified near-infrared (NIR) technique is adopted for the estimation of surface reflectance in *croplands*, which results from the excess gas absorption of the VIIRS band at 2.25 μm compared to the MODIS band at 2.12 μm; New non-spherical dust models are considered in DB_V to mitigate the discernible discontinuity of AOD spatial distribution in low-latitude areas caused by the forward and backward side-scattering direction. In our study, we consider the records of DB_M (C6.1) and DB_V with QA ≥ 2 over land as the appropriate data.

2.2.2.3. The VIIRS EDR AOD product. The EDR algorithm can generate the global and regional AOD products over both land and ocean, of

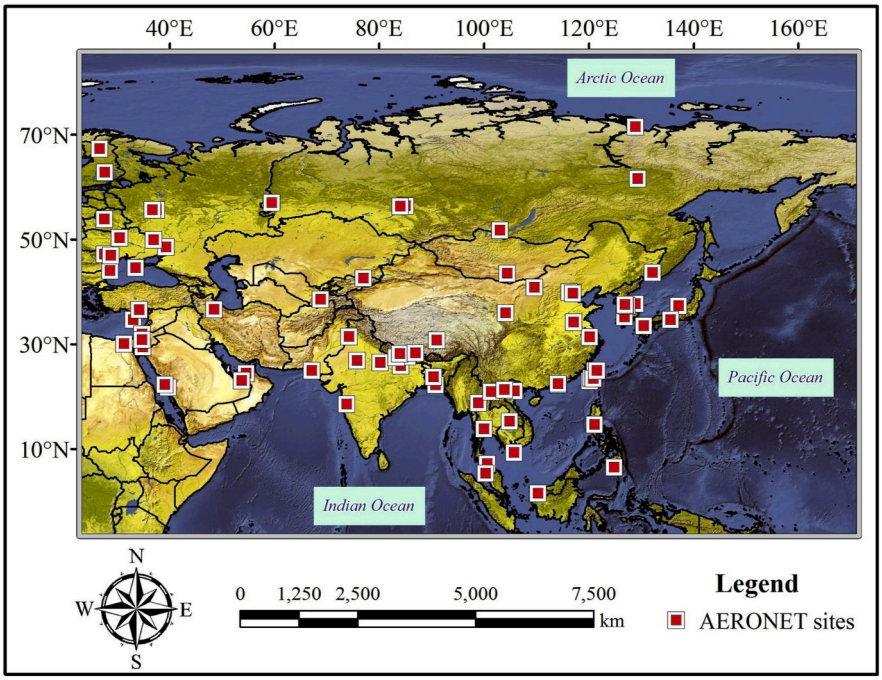

Fig. 1. The distribution of the AERONET sites in the study areas. The base-map in this figure is the natural earth shaded map.

which the procedures are similar to the DT algorithm (Jackson et al., 2013). For land, a total of three separate aerosol models based on geographic locations are assumed in this algorithm, including dust, low/high-absorption smoke, and clean/polluted urban. The regions over bright surface (high surface reflectance) and affected by cloud will be screened. In the EDR algorithm, the AOD values are retrieved using the LUT of a precomputed database for several atmospheric parameters to simplify the radiative transfer calculations. Meanwhile, the surface reflectance of the blue and red bands are estimated with the pre-determined relationships from that of the SWIR band. The AOD values are firstly acquired at the original spatial resolution of 750 m and then aggregated (8*8 pixels) to a coarser spatial resolution of 6 km. At last, the AOD values are stored at three levels for data quality: low (QA = 1), medium (QA = 2), and high (QA = 3). In our study, the record of EDR with the high level (QA = 3) over land is adopted.

2.2.3. MODIS land cover map

The MODIS land cover map (MCD12Q1) includes the datasets of global land cover classification in five different schemes (Al-Hamdan et al., 2014) at a 500-m spatial resolution and a 1-year temporal resolution, depicting the land cover properties originated from the combined Terra- and Aqua-MODIS observations. In our study, the first land cover scheme of MCD12Q1 is utilized, which contains the 17 land cover types defined by the International Geosphere Biosphere Programme (IGBP). For convenience, the specific types of land cover in Asia are simplified to six major types: *forest*, *savannas*, *grasslands*, *croplands*, *urban*, and *arid lands*. The details with respect to IGBP are illustrated in Fig. 2 (see specific types). In our study, the land cover map is remapped to the geographical projection (WGS84) of 0.005° × 0.005°using the nearest neighbor interpolation (Parker et al., 1983).

3. Evaluation and comparison results of the AOD products from MODIS and VIIRS

Generally, AERONET sites repeatedly provide the point-shaped measurements, while remote sensing sensors offer the AOD products of a certain spatial resolution at the overpass time. Therefore, the measurements of AERONET sites and the AOD products of remote sensing sensors are bound to be matched both spatially and temporally (Virtanen et al., 2018). In our study, the approach, which averages the AERONET measurements within an interval of ±30 min at the MODIS and VIIRS overpass time and the grids within a diameter of ~30 km (matching range) at each AERONET site center, is employed to obtain the matched points. The matching range is determined by calculation according to the parameters of WGS84 and the differences of longitude and latitude. Although AERONET sites acquire AOD measurements at diverse spectral bands, many of them are different from the MODIS (550 nm). Hence, the Ångström exponent (α) is utilized to calculate the true-values of AOD at 550 nm, which is defined as shown in Eq. (1).

$$\alpha = -\frac{\ln\left(\tau_1/\tau_2\right)}{\ln\left(\lambda_1/\lambda_2\right)} \tag{1}$$

where τ_1 and τ_2 represent the AOD at the spectral bands of λ_1 (440 nm) and λ_2 (870 nm), respectively. The results are evaluated with the expected error (EE), which is only based on the expected performance of DT over land (Levy et al., 2013), as shown in Eq. (2); the Pearson correlation coefficient (R); the root-mean-square error (RMSE), as shown in Eq. (3); the bias, as shown in Eq. (4); the mean absolute percentage error (MAPE), as shown in Eq. (5), and the relative mean bias (RMB), as shown in Eq. (6).

$$\mathrm{EE} = \pm\left(0.05 + 0.15 \times \tau_{AERO}\right) \tag{2}$$

$$\mathrm{RMSE} = \sqrt{\frac{1}{n}\sum_{i=1}^{n}\left(\tau_{(SEN)i} - \tau_{(AERO)i}\right)^2} \tag{3}$$

$$\mathrm{Bias} = \frac{1}{n}\sum_{i=1}^{n}\left(\tau_{(SEN)i} - \tau_{(AERO)i}\right) \tag{4}$$

$$\mathrm{MAPE} = \frac{1}{n}\sum_{i=1}^{n}\frac{\left|\tau_{(SEN)i} - \tau_{(AERO)i}\right|}{\tau_{(AERO)i}} \tag{5}$$

$$\mathrm{RMB} = \frac{\sum_{i=1}^{n}\tau_{(SEN)i}}{\sum_{i=1}^{n}\tau_{(AERO)i}} \tag{6}$$

where τ_{SEN} and τ_{AERO} denote the AOD from remote sensing sensors (MODIS and VIIRS) and AERONET sites, respectively.

3.1. Evaluation and comparison of DB_M, DT, DB_V, and EDR according to aerosol loadings

As demonstrated in Fig. 3, the AOD products of DB_M, DT, DB_V, and EDR are evaluated for a total of 16,654, 11,580, 15,270, and 15,948 matched points in Asia, respectively. Overall, the AOD product of DB_V achieves the best performance, with the R of 0.91 and the RMSE of 0.14. At the same time, the performance of DB_M and DT are acceptable, with similar metrics. On the contrary, the AOD quality of EDR is considered poor, of which the fraction within the EE is only 55.05%. For the EDR algorithm, the AOD range used in the LUT is [0, 2] (Jackson et al., 2013)

No.	Areas percentage	Specific types	Major types
1	1.65%	Evergreen needleleaf forest	
2	3.20%	Evergreen broadleaf forest	
3	0.82%	Deciduous needleleaf forest	*Forest*
4	2.35%	Deciduous broadleaf forest	
5	5.91%	Mixed forest	
6	0.17%	Closed shrublands	-
7	8.02%	Open shrublands	-
8	9.04%	Woody savannas	*Savannas*
9	9.06%	Savannas	
10	23.62%	Grasslands	*Grasslands*
11	1.05%	Permanent wetlands	-
12	12.51%	Croplands	*Croplands*
13	0.69%	Urban and built-up	*Urban*
14	1.10%	Cropland/natural vegetation mosaic	*Croplands*
15	0.26%	Snow and ice	-
16	20.56%	Barren or sparsely vegetated	*Arid lands*

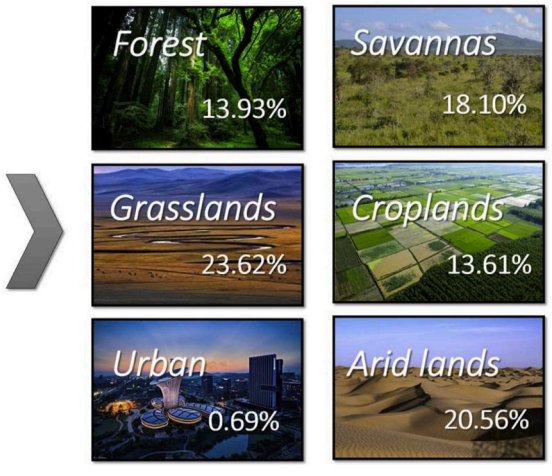

Fig. 2. The land cover types of the study areas. In the right part, the number represents the area percentage of each major land cover type.

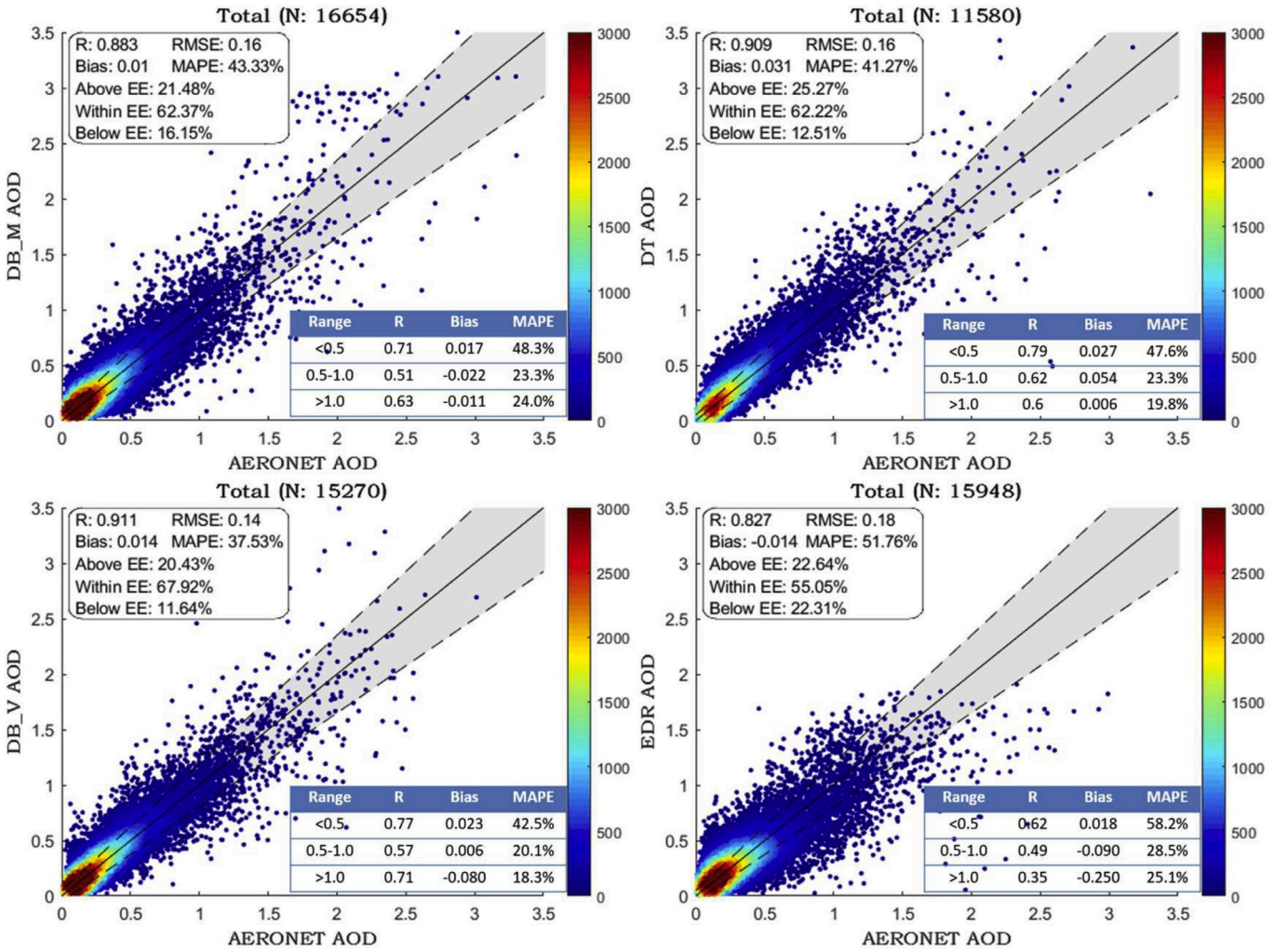

Fig. 3. The evaluation results (scatter plots and tables) of DB_M, DT, DB_V, and EDR against AERONET. In the scatter plots, the black solid line represents the standard line (1:1), the dash lines denote the EE lines, and the range of EE is painted with the shade of light gray. The tables show some metrics for different aerosol loadings and the color bars illustrate the count of matched points within a radius of 0.1 (AOD). (For interpretation of the references to color in this figure legend, the reader is referred to the Web version of this article.)

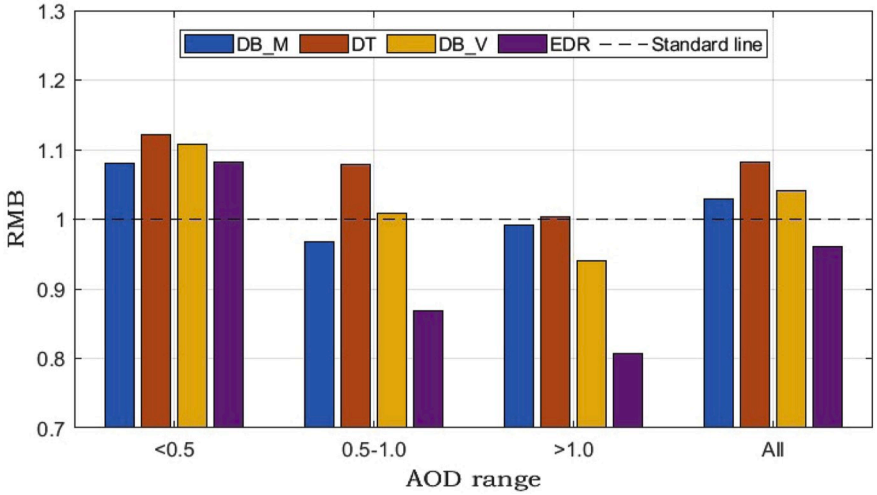

Fig. 4. The RMBs for DB_M, DT, DB_V, and EDR against AERONET for different aerosol loadings.

and consequently a large underestimation will emerge at the AOD values of more than 2, which is also reflected in Fig. 3. For diverse aerosol loadings (see tables in Fig. 3), it's discovered that the MAPEs for all AOD products are much larger at the AOD values of less than 0.5 compared to those at other ranges. Therefore, the uncertainty of each AOD product from DB_M, DT, DB_V, and EDR is supposed to contain a constant deviation, which doesn't change with the variation of AOD values and is also reflected in Eq. (2). Meanwhile, it's found that the Rs and the MAPEs for DB_V during all aerosol loadings are better than those for DB_M, indicating that the improvements in the DB_V algorithm are effective. In addition, as depicted in Fig. 4, all AOD products will generally overestimate the AOD values at the numbers of less than 0.5. Especially, an obvious underestimation is observed in EDR when the AOD values exceed 0.5.

Next, the deviations distribution for all AOD products is presented in Fig. 5, in the form of box plots. To be specific, the matched points are sorted in the ascending order of the AERONET AOD values and then sampled with a fixed interval, which could generate 80 boxes for each AOD product of DB_M, DT, DB_V, and EDR, respectively. Overall, the boxes showing the deviations for DB_M, DT, and DB_V remain well within the EE lines following the increment of the aerosol loadings. The deviations distribution for DB_M and DB_V are small, while the deviations ranges for DB_V between the whisker vertexes are shorter, suggesting better performance. For the AOD product of DT, a slight overestimation is observed in almost all AOD values, which is likely caused by the inaccurate assumptions in aerosol models and surface reflectance (Bilal et al., 2014, 2016; He et al., 2010; Wang et al., 2019a). With regard to EDR. it's discovered that the boxes decline as the AOD values rise and exceed the EE lines at the numbers of more than 0.5, requiring improvements. The frequency distribution of DB_M, DT, DB_V, and EDR is illustrated in Fig. 6. The x axis is truncated at 2 since the percentages that the AOD values exceed 2 are less than 7‰ for all AOD products. As can be seen, the frequency of all AOD products differs from AERONET with diverse levels, which change with the variation of AOD ranges. From Fig. 6, the frequency distribution of DB_M is generally the closest to AERONET. However, the AOD product of DT shows a large difference of frequency at the AOD values of less than 0.2 compared to AERONET. Meanwhile, the frequency of DT is always larger than that of AERONET when the AOD values exceed 0.3. It can be inferred that the large difference between DT and AEROENT at the AOD values of less than 0.2 likely results from the overestimation of DT. The frequency distribution of DB_V is similar with DB_M, with the frequency difference of less than 0.02 for all AOD ranges. With regard to EDR, which is developed based on DT (Jackson et al., 2013), the frequency distribution is different from that of DT. It can be observed that the difference between EDR and AEROENT at the AOD values of less than 0.2 is smaller

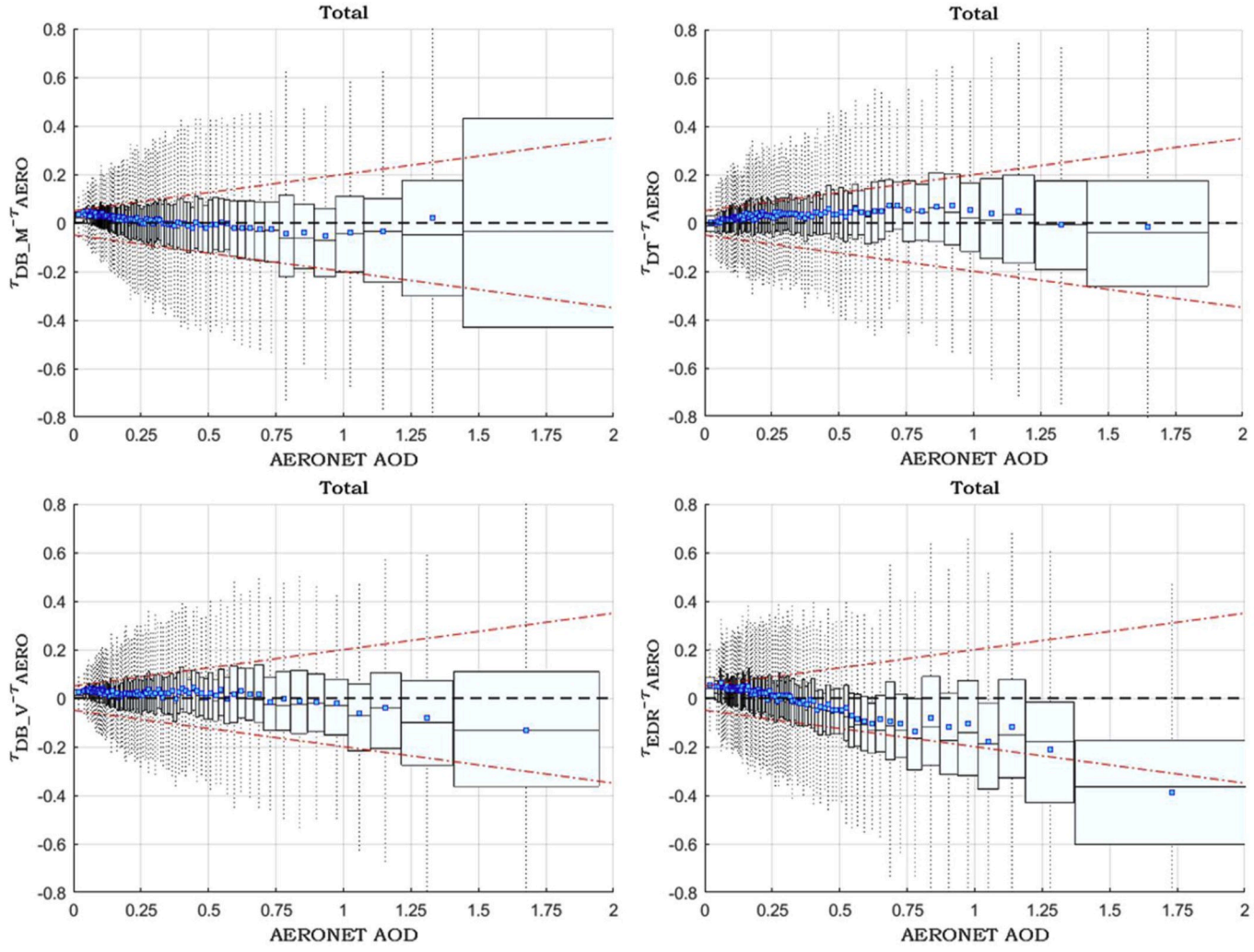

Fig. 5. The evaluation results (box plots) of DB_M, DT, DB_V, and EDR against AERONET. The black horizontal dash line denotes the zero-line and the red dot dash lines represent the EE lines. For each box, the middle line, azure dot, top and bottom hinges, and whisker vertexes are the median, mean, 25th and 75th percentiles, and 1.5 times the interquartile range (IQR) of AOD deviations, respectively. τ: AOD. (For interpretation of the references to color in this figure legend, the reader is referred to the Web version of this article.)

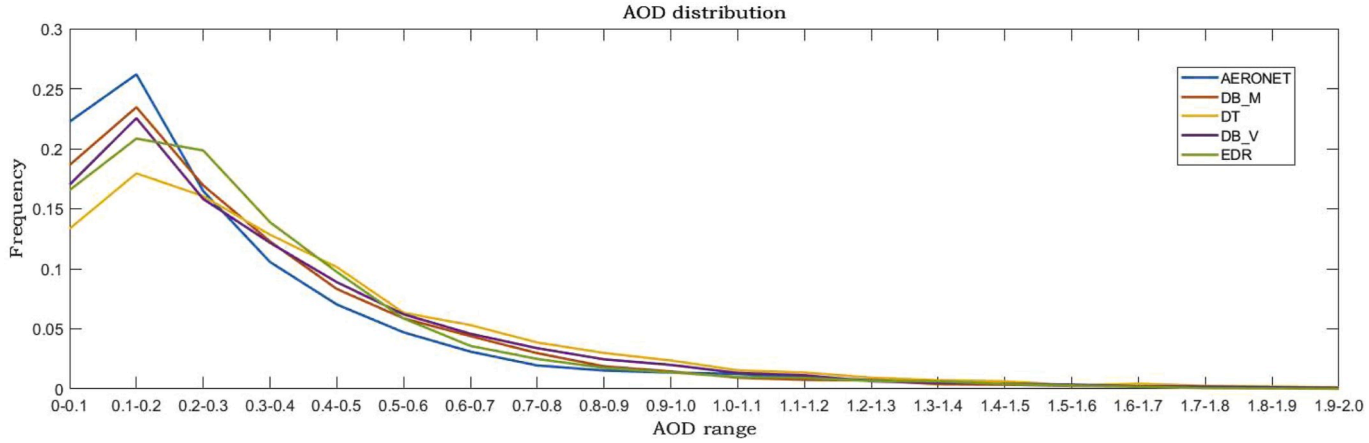

Fig. 6. The frequency distribution of AERONET, DB_M, DT, DB_V, and EDR. The negative AOD values of DT (down to −0.05) are discarded.

compared to DT.

3.2. Evaluation and comparison of DB_M, DT, DB_V, and EDR according to temporal sequence

At first, the time series and annual cycle for DB_M, DT, DB_V, and EDR are displayed in Fig. 7 to show the variation of deviations between each AOD product and AERONET with the change of time. From Fig. 7 (top), the deviations for DB_M, DT, DB_V, and EDR fluctuate with different levels as time moves forward. Generally, the AOD product of DB_V overcomes others with the smallest overall deviation. Meanwhile, the largest positive and negative deviations are observed in DT and EDR, respectively. It's discovered that the variation of deviations for each AOD product is periodic, which is obviously reflected in the annual cycle plot. As shown in Fig. 7 (bottom), the deviations for DT and EDR is considered large and greatly differs from that for DB_M and DB_V in serval months. It's clear that significant deviations mainly exist in the period of May to Jul for DT and Nov to Mar for EDR, respectively. This likely results from the inaccurate suppositions of aerosol models and surface reflectance for DT and EDR in these months (Bilal et al., 2014, 2016; He et al., 2010; Wang et al., 2019a).

Previously, it's has been discovered that the performance of AOD products is related to the significant seasonality (Mhawish et al., 2017, 2019), which inspires us to compare DB_M, DT, DB_V, and EDR in

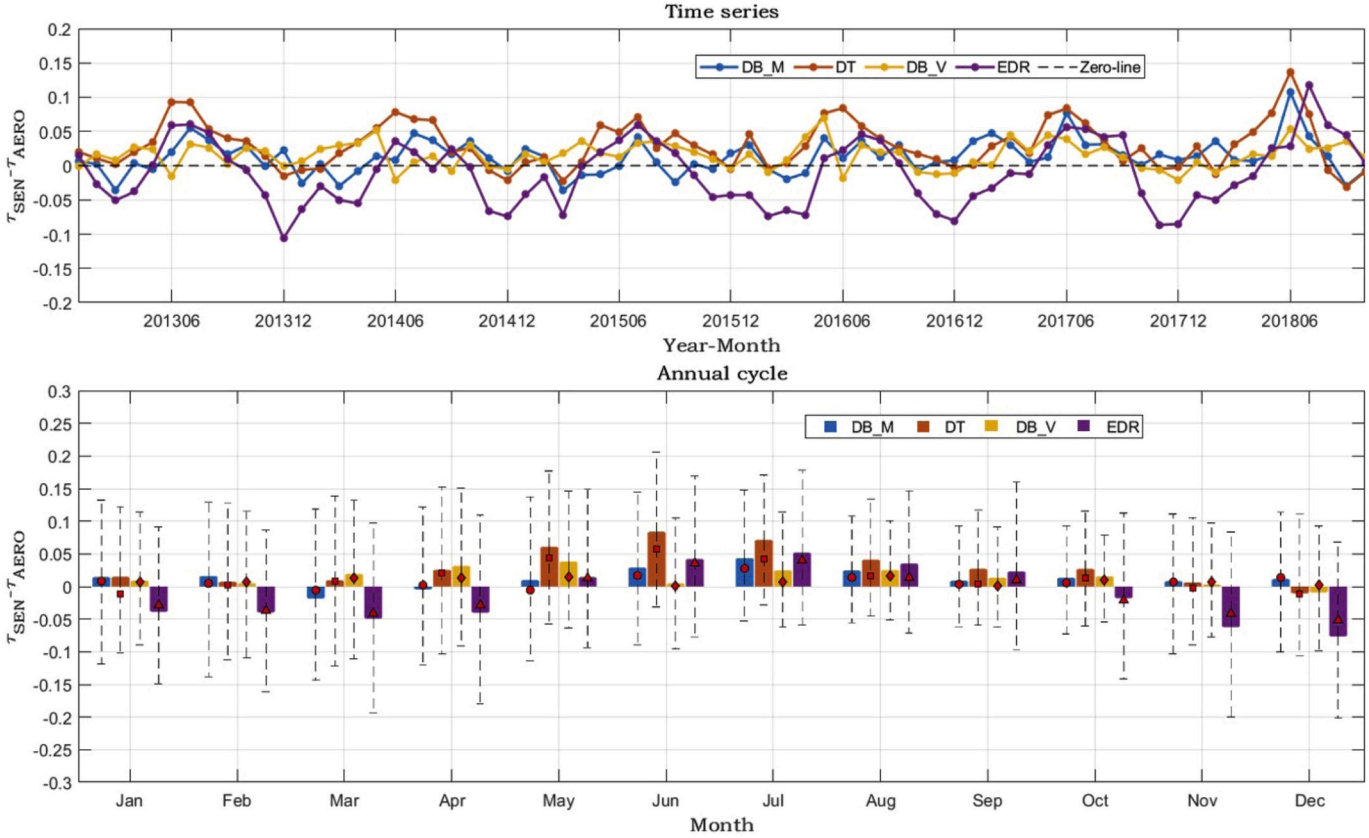

Fig. 7. Time series and annual cycle of the deviations of DB_M, DT, DB_V, and EDR against AERONET. In the annual cycle plot, the bars represent the means, the red marks denote the medians, and the ranges of dash lines include 68% of the data. τ: AOD. (For interpretation of the references to color in this figure legend, the reader is referred to the Web version of this article.)

different seasons. In our study, the months throughout one year are divided into four seasons: DJF (Dec., Jan., and Feb.), MAM (Mar., Apr., and May.), JJA (Jun., Jul., Aug.), and SON (Sep., Oct., and Nov.). As can be seen from Table 1, each AOD product achieves different performance with the variation of seasons. For DJF, the surface reflectance likely increases in vegetation regions (Canisius et al., 2007; Wang et al., 2014) and also in *urban* (Li et al., 2012). As a result, the number of matched points for DT is significantly less than that for DB_M and DB_V in DJF due to the bright surface. On the contrary, the number of matched points for EDR is still considerable, while the AOD quality is worse with the R of 0.853 and the bias of −0.049, respectively. The distinction of the matched points number and the AOD quality may be caused by the different procedures and the QA criteria in the DT and EDR algorithms (Gupta et al., 2016; Jackson et al., 2013). With regard to JJA, more cloud exists in the South (except the *arid lands*) with the increment of temperature compared to other seasons (see a case of 2018 in Fig. s1 from the supplementary materials). It's observed that the MAPEs are poor for all AOD products in JJA and the RMBs also exceeds 1 (especially for DT), which likely results from the inaccurate assumptions in AOD retrieval algorithms (Bilal et al., 2014, 2016; He et al., 2010; Wang et al., 2019a) and the leak detections in cloud masks (Gupta et al., 2016; Wang et al., 2019a; Hsu et al., 2019; Jackson et al., 2013). In addition, it's found that the fractions within EE and the MAPEs for DB_V in the four seasons are better than those for DB_M, further suggesting the effectiveness of the improvements in the DB_V algorithm.

3.3. Evaluation and comparison of DB_M, DT, DB_V, and EDR according to AOD-related factors

The AOD-related factors are of great importance for retrieving AOD products. For instance, the methods of surface reflectance estimations in the DB algorithm are hybrid based on the land cover types (Hsu et al., 2019); The aerosol models in the DT algorithm are dynamic and blend two modes: coarse particles and fine particles (Gupta et al., 2016). Hence, it is instrumental to consider these factors in the procedures of evaluation and comparison.

The first AOD-related factor that our study considers is the land cover types. The ratio of each land cover type in the matching range (~30 km) is calculated and only the type of which the ratio exceeds 80% will be deemed as a single type. As demonstrated in Fig. 8, the performance of each AOD product is different in the regions with diverse land cover types. For *forest*, the Rs for the AOD products of DB_M, DT, DB_V, and EDR all exceed 0.9, suggesting good correlations with the AERONET. However, as shown in Fig. 9, the RMBs of them are less than 1, which means that all AOD products will generally underestimate the AOD values in *forest*. Taking all metrics into account, DT outperforms other AOD products in *forest*, with the smallest bias, the largest RMB, and the largest fraction within EE. Similar to *forest*, the AOD products of DB_M, DT, DB_V, and EDR show high correlations with the AERONET in *savannas*, while underestimations are also discovered. In Asia, the regions of *grasslands* usually distribute in the plateaus with high elevation. As can be seen, the Rs for DT and EDR are much poorer than those for DB_M and DB_V, indicating that the surface reflectance estimations and the aerosol models hypotheses of DT and EDR may be not appropriate (Bilal et al., 2014, 2016; He et al., 2010; Wang et al., 2019a) in *grasslands*. It's worth mentioning that the RMB for DT is significantly larger compared to other AOD products and greatly exceeds 1, which further indicates that serious issues likely exist in DT for *grasslands*. On the contrary, DB_V achieves the best performance in *grasslands* with the R of 0.935 and the fraction within EE of 78.54%. As for *croplands*, a modified NIR technique is adopted for the surface reflectance estimations in the DB_V algorithm (Hsu et al., 2019). Therefore, it's clear that DB_V performs better than DB_M in *croplands*, reflected in the metrics of the RMSEs, the MAPEs, and the fractions within EE. The accuracy of AOD products in *urban* is of great importance and widely receives attention from scholars (Kaskaoutis et al., 2009; Kharol et al., 2011; Wang et al., 2015). From Fig. 9, it's found that the AOD products of DB_M, DT, and EDR will universally overestimate the AOD values in *urban*, especially for DT and EDR. Actually, in the C6.1 DT algorithm, the method of surface reflectance estimations in *urban* has been modified with the urban percentage (Gupta et al., 2016). Meanwhile, the modification has been also effectively evaluated in Beijing (Bilal et al., 2019; Tian et al., 2018; Wang et al., 2019a). However, the overestimation of DT is still considerable in *urban* over Asia at the urban percentage exceeds 80%, requiring further improvements. In *urban*, there is no doubt that the performance of DB_V is the best, with the R of 0.965 and the RMSE of 0.12. Considering the fact that DT and EDR are not devised for bright surface, only DB_M and DB_V will be evaluated in *arid lands*. In the DB_V algorithm, the new non-spherical dust models are used to mitigate the discernible discontinuity of AOD spatial distribution in low-latitude areas (Hsu et al., 2019). As illustrated in Figs. 8 and 9, the R for DB_V exceeds that for DB_M in *arid lands*, while the bias and the RMB for DB_V are poorer, indicating that larger overestimation exists in DB_V.

Next, considering the fact that aerosol columns are optically dominated by coarse particles ($AE_{440\text{-}870} \leq 0.7$), mixed distributions ($0.7 < AE_{440\text{-}870} \leq 1.3$), and fine particles ($AE_{440\text{-}870} > 1.3$) (Mhawish et al., 2017, 2019; Sayer et al., 2014), the aerosol particles are categorized into these three types for further analyses. As depicted in Fig. 10, fine particles are the major aerosol particles in *forest*, with the largest proportion. Meanwhile, it's obvious that a great overestimation in DB_M exists compared to other AOD products when the $AE_{440\text{-}870}$ exceeds 1.3, which denotes that the aerosol models of fine particles assumed for DB_M are may be inexact in *forest*. Similarly, for *savannas*, fine particles are also the primary aerosol particles, while significant underestimations are mainly observed in DB_M and EDR during the fine particles. With regard to *grasslands*, the variation trends of deviations for DB_M and DB_V are relatively stable by comparison to DT and EDR. To be specific, an overestimation and underestimation are generally discovered during

Table 1
The evaluation results of DB_M, DT, DB_V, and EDR against AERONET in different seasons. τ_A: the AOD from AERONET sites.

Season	N				R				Bias			
	DB_M	DT	DB_V	EDR	DB_M	DT	DB_V	EDR	DB_M	DT	DB_V	EDR
DJF	4206	2281	4145	3663	0.870	0.893	0.906	0.853	0.013	0.005	0.002	−0.049
MAM	5359	4093	4940	4977	0.880	0.899	0.904	0.822	−0.005	0.031	0.028	−0.024
JJA	3074	2542	2284	3587	0.899	0.932	0.893	0.811	0.031	0.065	0.016	0.042
SON	4015	2664	3901	3721	0.907	0.921	0.930	0.830	0.009	0.020	0.010	−0.018
Season	MAPE (%)				Within EE (%)				RMB			
	DB_M	DT	DB_V	EDR	DB_M	DT	DB_V	EDR	DB_M	DT	DB_V	EDR
DJF	46.23	34.38	37.49	48.68	55.75	63.79	64.85	54.98	1.04	1.01	1.00	0.88
MAM	38.78	38.60	37.36	41.04	60.87	58.29	64.92	56.66	0.99	1.07	1.07	0.94
JJA	49.34	50.97	42.14	65.09	64.83	60.35	68.30	55.20	1.11	1.22	1.06	1.16
SON	41.75	42.03	35.09	56.30	69.41	68.69	74.78	52.84	1.03	1.06	1.03	0.94

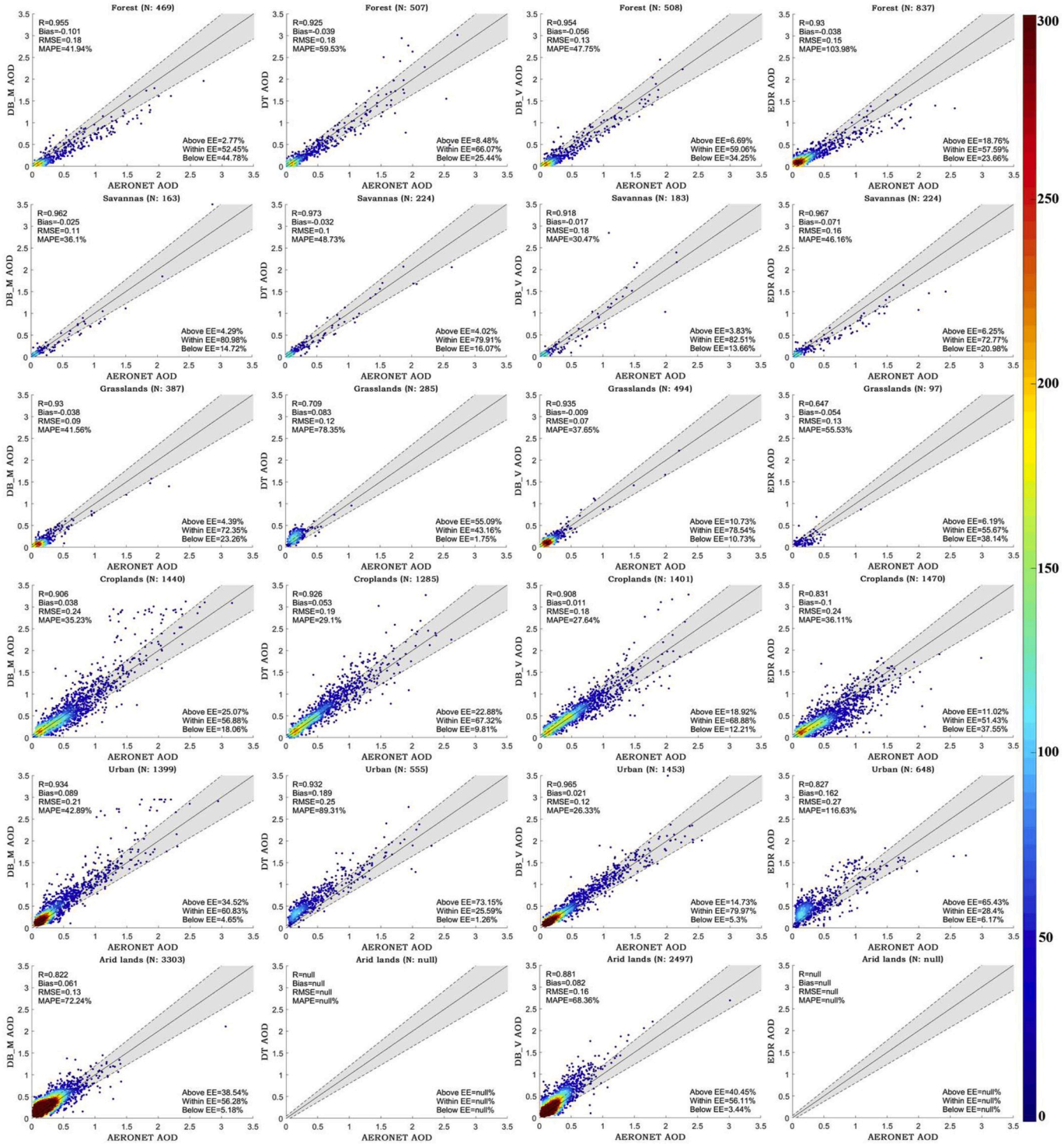

Fig. 8. The evaluation results (scatter plots) of DB_M, DT, DB_V, and EDR against AERONET for diverse land cover types. The black solid line represents the standard line (1:1), the dash lines denote the EE lines, and the range of EE is painted with the shade of light gray. The color bar illustrates the count of matched points within a radius of 0.1 (AOD). (For interpretation of the references to color in this figure legend, the reader is referred to the Web version of this article.)

almost all aerosol particles in *grasslands* for DT and EDR, respectively. As mentioned above, a modified NIR technique of DB_V is adopted for the surface reflectance estimations in *cropland* (Hsu et al., 2019). As a result, from Fig. 10, the box sizes for DB_V are smaller than those for DB_M during all aerosol particles in *croplands*, also suggesting the better performance. It's found that a visible underestimation emerges in EDR during coarse particles and mixed distributions in *croplands*, requiring further improvements of aerosol models for it. As for *urban*, the AOD products of DB_M, DT, and EDR except DB_V will generally overestimate the AOD values during all aerosol particles. In *arid lands*, it's known that the new non-spherical dust models are used to mitigate the discernible discontinuity of AOD spatial distribution for DB_V in low-latitude areas (Hsu et al., 2019). Surprisingly, a larger overestimation emerges in DB_V compared to DB_M during coarse particles, which likely means that the new dust models are improvable and need modifications in *arid lands*.

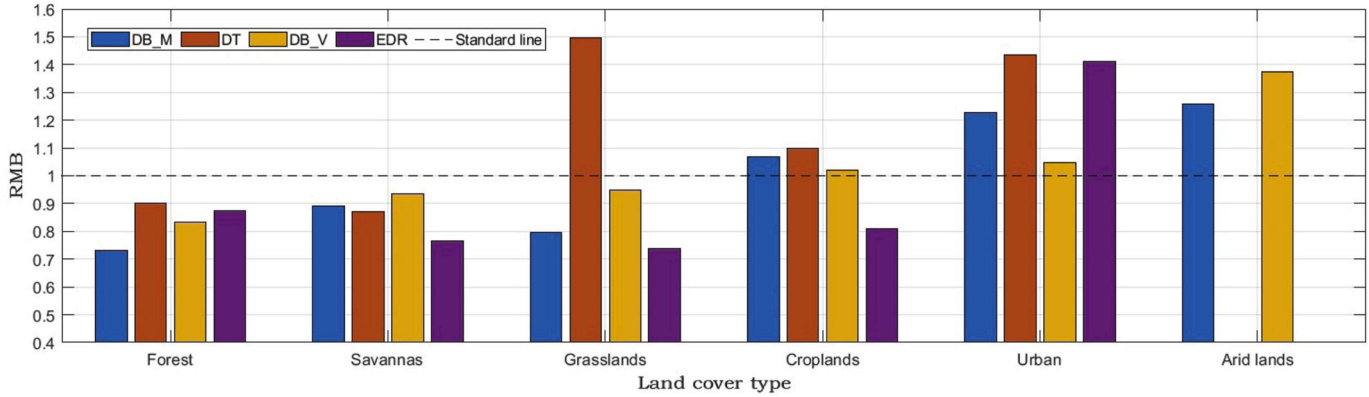

Fig. 9. The RMBs for DB_M, DT, DB_V, and EDR against AERONET for diverse land cover types.

4. Analyses of AOD spatiotemporal distribution and AOD completeness

In the past, the researches about the seasonal AOD spatial distribution are always hot topics (Della Ceca, 2018; He et al., 2016; Mhawish et al., 2017, 2019). In our study, the AOD products of DB_M, DT, DB_V, and EDR in each season during 2013–2018 are averaged to show the seasonal AOD spatial distribution in Fig. 11. As can be seen, the AOD values of DB_M, DT, DB_V, and EDR are missing in the North due to the long-time series of snow cover in DJF. Even in MAM, the AOD values are still invalid caused by the same reason when the latitudes exceed 70°. For JJA, the AOD coverage of them is much increased in the North. Surprisingly, the valid AOD values of EDR are absent at the latitudes of more than 70°in SON, likely resulting from the small threshold of dark surface recognition or the QA filter in the algorithm (Jackson et al., 2013). The distribution of high AOD values for DT and EDR shows difference in four seasons, which is dominated by multiple factors, such as anthropogenic activities. With regard to DB_M and DB_V, apart from the seasonal variations, the high AOD values also distribute in *arid lands* in MAM and JJA. Meanwhile, the seasonal AOD value of DB_V is usually larger than that of DB_M in these seasons (MAM and JJA) over bright surface, especially the deserts in Asia. This discovery further indicates that the new dust models are improvable and modifications are required for DB_V in *arid lands*, which has been mentioned in Section 3.3. Except for the bright surface, the seasonal AOD spatial distribution is similar for the AOD products of DB_M, DT, DB_V, and EDR. For all seasons, the valid AOD values of DB_M and DB_V distribute in most of the study areas, except some regions with the year-round snow cover. Nevertheless, a long-term (2013–2018) absence of valid AOD values for DT and EDR can be observed in the regions over bright surface, such as the Takla Makan Desert and Saudi Arabia.

Generally, the seasonal AOD spatial distribution shows significant difference, which is related to the land cover types of the underlying surface. For instance, the AOD values of MAM and JJA tend to be larger than those of DJF and SON in *arid lands*. Although the quality of each AOD product is different, yet the seasonal variation trends of AOD values should be similar for the same land cover type. Otherwise, the unique seasonal variation trends would indirectly suggest the distribution of AOD values far from other AOD products in this land cover type. To analyze this issue, the statistical charts of all AOD products for diverse land cover types in different seasons are presented in Fig. 12. The simplified land cover types at the spatial resolution of $0.005° \times 0.005°$are aggregated to $0.1° \times 0.1°$and $0.06° \times 0.06°$to be consistent with the AOD products (only the type of which the ratio exceeds 80% in the grids will be considered as a single type). As can be observed, some seasonal variation trends of DB_M, DT, DB_V, and EDR are similar for one land cover type with a slight discrepancy, such as *forest* and *savannas*. Nevertheless, the seasonal variation trends of DT and EDR greatly differ from those for DB_M and DB_V for *grasslands*. As described in Section 3.3, the performance of DT and EDR is much worse compared to DB_M and DB_V in *grasslands*. Meanwhile, the update of DB_V is reflected in Fig. 12d for *croplands* as well. The distinctions of seasonal variation trends can be discovered for *urban* (e.g., larger overestimation in DT) and *arid lands* (e.g., larger overestimation in DB_V), which are also consistent with the analyses in Section 3.3.

In addition to the AOD spatial distribution, the completeness of valid AOD values is also one of the hot spots for the scientific community (He et al., 2017; Liu et al., 2019; Wang et al., 2019a). The annual AOD completeness, i.e., the percentage of valid AOD values in each grid during 2013–2018, of DB_M, DT, DB_V, and EDR is mapped in Fig. 13. It's well known that the AOD completeness of all AOD products is mainly affected by the contaminations from cloud and snow cover. As shown in Fig. 13, the small annual AOD completeness of them usually distributes in the North and Tibet due to more cloud and snow cover (see a case of 2018 in Fig. s2 from the supplementary materials). For DB_M and DB_V, the annual AOD completeness tends to be large in the Southwest, where the major land cover type is *arid lands*. It's obvious that *arid lands* are often lack of moisture compared to other regions and consequently the probability of cloud emerging significantly decreases (Wang et al., 2019a). The regions, where the annual AOD completeness of DB_V exceeds that of DB_M, largely distribute in the north of India as expected (no scanning gaps between two adjacent orbits in low-latitude areas like MODIS). However, the annual AOD completeness of DB_M is still larger than that of DB_V in many other regions (especially the *arid lands*). This likely results from some distinctions in the DB_M and DB_V algorithms, such as the aerosol models, wavelengths of spectral bands used to retrieve AOD values, and sensor zenith angle ranges. Furthermore, it's worth noting that the overlap regions are only filled with the swath at the maximum overpass time in our study. In other words, the AOD completeness will increase provided that all the swaths in the overlap regions are utilized, particularly for VIIRS due to the wider swath width compared to MODIS (Sayer et al., 2019). Nevertheless, this circumstance is not adopted and discussed in this paper. As for DT and EDR, the large annual AOD completeness principally distributes in India, where the primary land cover type is *croplands*. A comparison of the average AOD completeness in the study areas for DB_M, DT, DB_V, and EDR is then made according to different seasons. As listed in Table 2, the largest average AOD completeness is observed in DB_M for annual and four seasons. Meanwhile, the variations of the average seasonal AOD completeness are diverse for the AOD products of DB_M, DT, DB_V, and EDR. For instance, the largest average seasonal AOD completeness exists in SON for DB_M and DB_V but in JJA for DT and EDR.

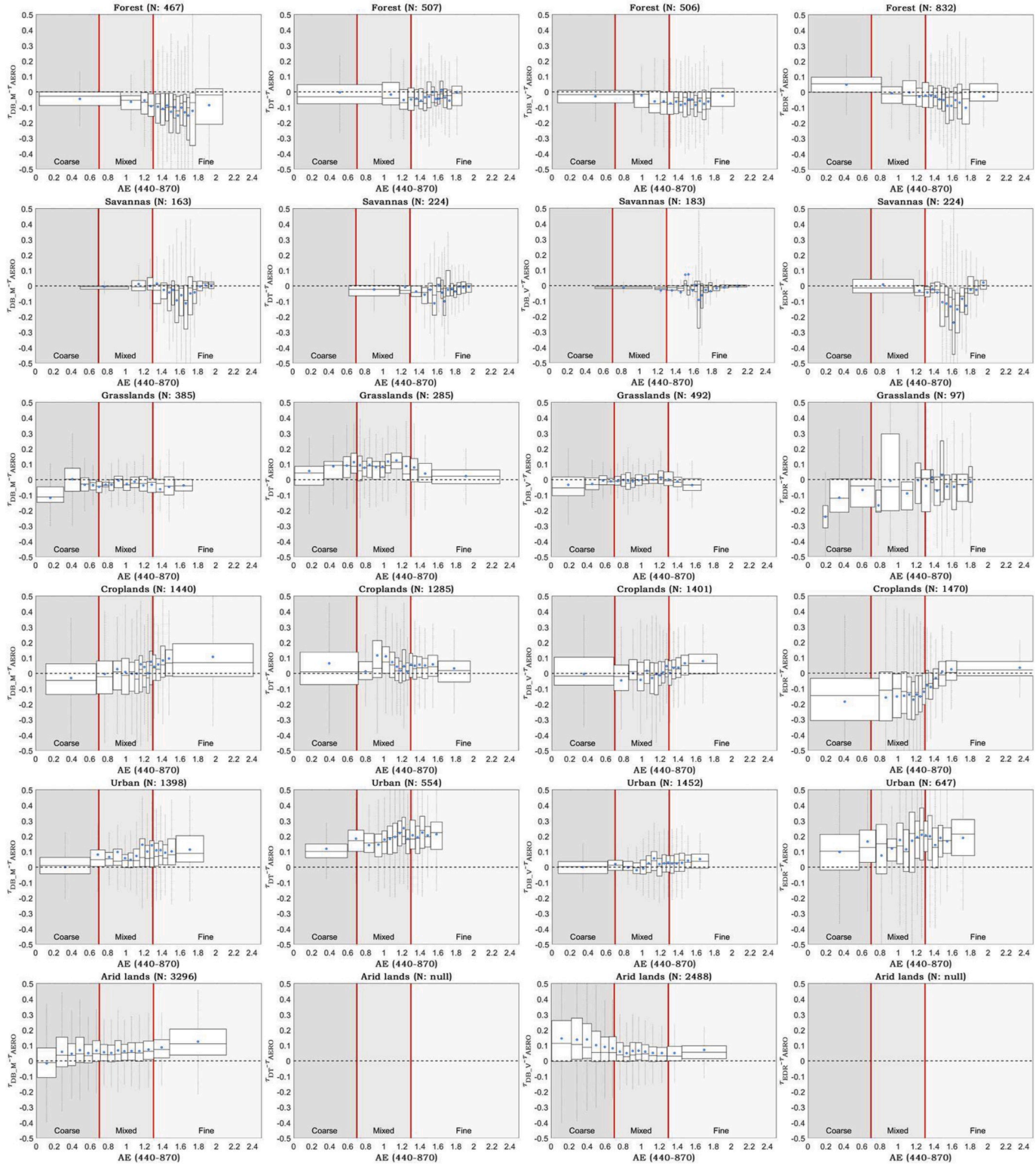

Fig. 10. The evaluation results (box plots) of DB_M, DT, DB_V, and EDR against AERONET for diverse land cover types considering different aerosol particles. The black horizontal dash line denotes the zero-line and the red solid lines represent the demarcation lines for different aerosol particles, where are painted with three shades of gray. For each box, the middle line, azure dot, top and bottom hinges, and whisker vertexes are the median, mean, 25th and 75th percentiles, and 1.5 times the interquartile range (IQR) of AOD deviations, respectively. τ: AOD. (For interpretation of the references to color in this figure legend, the reader is referred to the Web version of this article.)

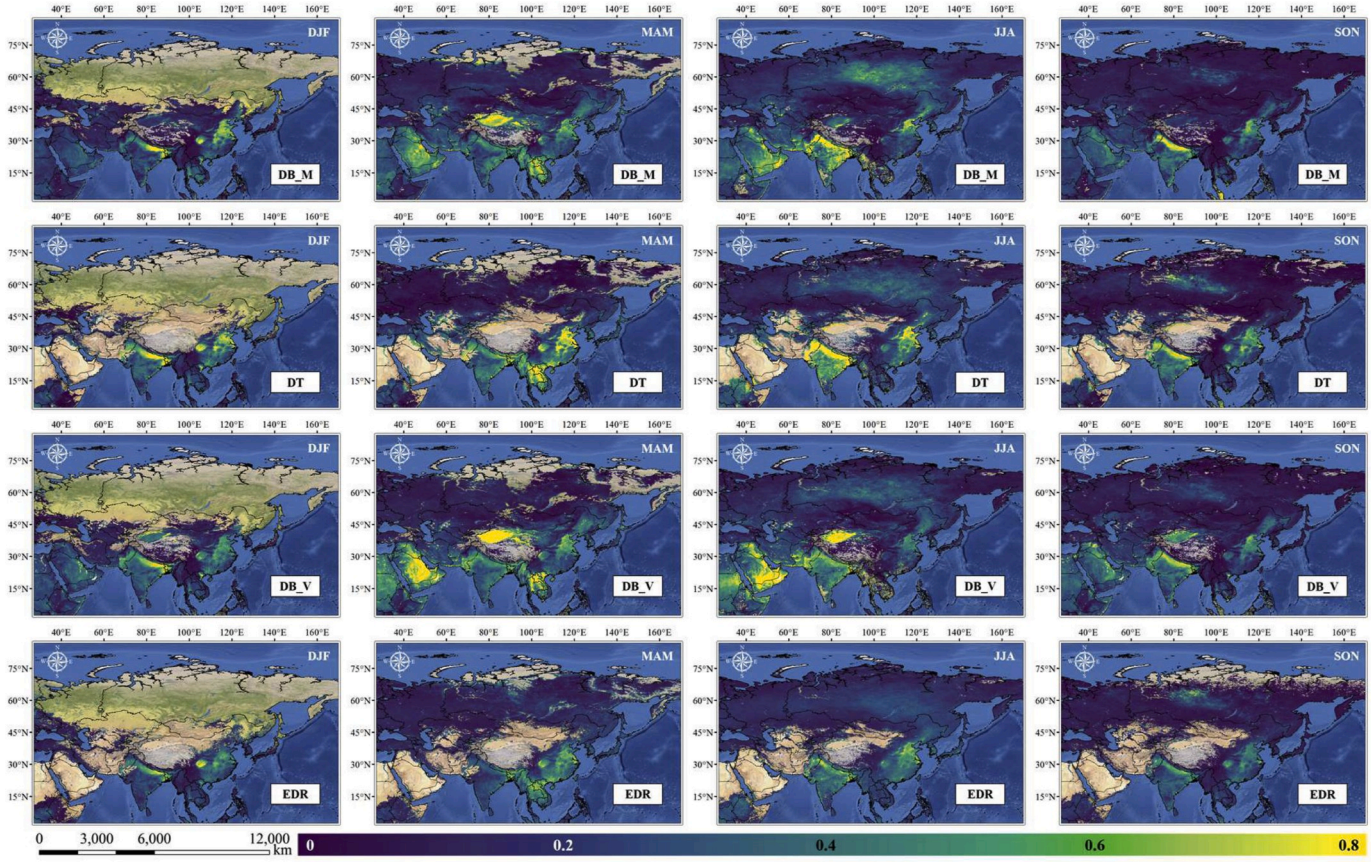

Fig. 11. The seasonal AOD spatial distribution of DB_M, DT, DB_V, and EDR during 2013–2018. The base-map in this figure is the natural earth shaded map and the color bar illustrates the AOD values. (For interpretation of the references to color in this figure legend, the reader is referred to the Web version of this article.)

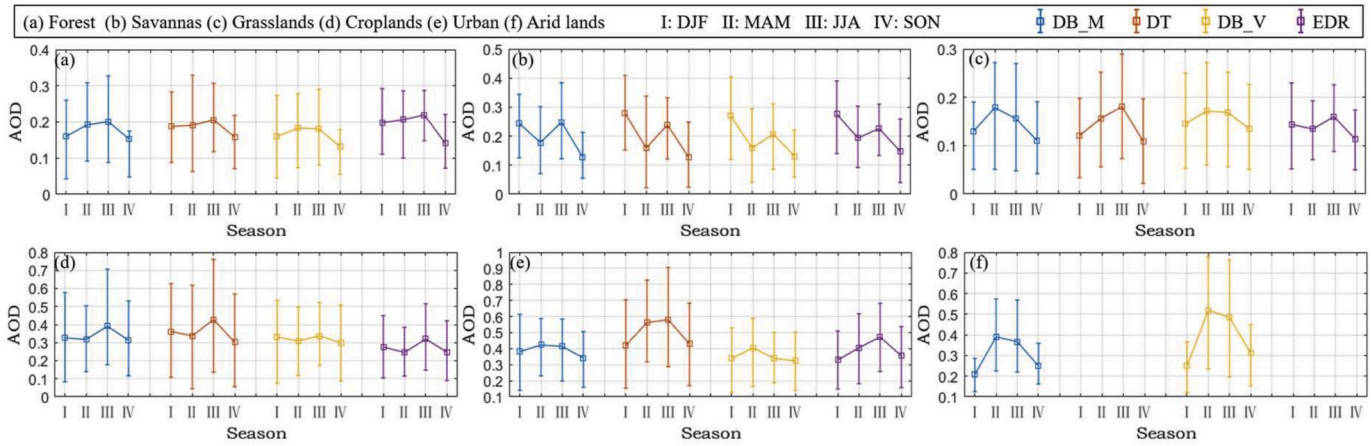

Fig. 12. The statistical charts of DB_M, DT, DB_V, and EDR for diverse land cover types in different seasons. The hollow marks represent the means and the ranges of solid lines include 68% of the data.

5. Merging of the AOD products from MODIS and VIIRS

5.1. Methodology

To date, numerous works have spared no effort to merge multiple AOD products (Bilal et al., 2017; Tang et al., 2016; Wang et al., 2019b). As is known to us from the previous sections, the AOD products of DB_M, DT, DB_V, and EDR show the different performance and AOD completeness. This is deemed as a good potential for merging, which could acquire the AOD product with the best performance and the largest AOD completeness as much as possible. In conclusion, a novel grid-based merging framework (SL-SGW) is proposed in our study, inspired by the methods of evaluation and comparison. It's worth noting that all AOD products, AERONET measurements, land cover types, etc. during 2013–2016 are employed to establish the merging framework, while the datasets during 2017–2018 are used to evaluate the merged AOD product.

As demonstrated in the flowchart (Fig. 14), the AOD products of DB_M, DT, DB_V, and EDR and the AERONET measurements (2013–2016) are firstly matched with the approaches described in

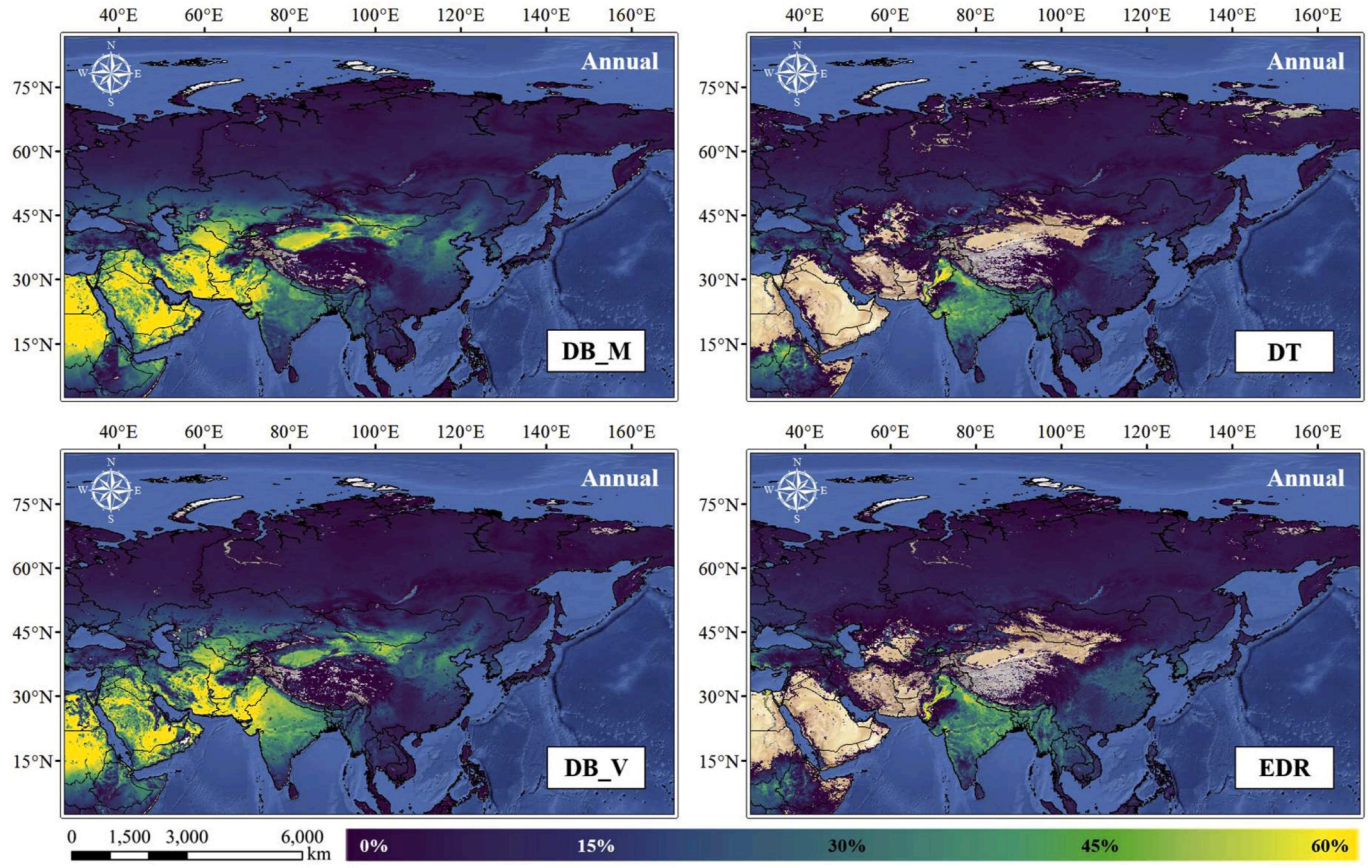

Fig. 13. The annual AOD completeness of DB_M, DT, DB_V, and EDR during 2013–2018. The base-map in this figure is the natural earth shaded map and the color bar illustrates the AOD completeness. (For interpretation of the references to color in this figure legend, the reader is referred to the Web version of this article.)

Table 2
The average AOD completeness of DB_M, DT, DB_V, and EDR during for annual and different seasons.

Name	Annual	DJF	MAM	JJA	SON
DB_M	20.84%	19.82%	19.21%	21.24%	23.11%
DT	8.09%	7.41%	7.65%	9.23%	8.05%
DB_V	18.71%	18.62%	18.08%	17.71%	20.44%
EDR	8.51%	7.81%	7.94%	10.49%	7.74%

Section 3 for different seasons and diverse land cover types. Next, the improvable AOD products (for each season and land cover type) will be selected to calculate the correction parameters of themselves with the polynomial fitting as Eq. (7).

$$\tau_{AERO} = \sum_{i=0}^{n} A_i \tau_{SEN}^{i} \tag{7}$$

where τ_{SEN} and τ_{AERO} denote the AOD from remote sensing sensors (MODIS and VIIRS) and AERONET sites, respectively; A represents the correction parameters. The list of correctable AOD products is provided in the supplementary materials (Table s2). After correction, the AOD products for each season and each land cover type will be sorted according to the performance and deemed as the sequence template (see Table s3 in the supplementary materials) for merging. When the sequence template is completed, the datasets during 2017–2018 could be utilized to validate the merging framework. First of all, the AOD products of DB_M and DT should be resampled to 0.06°with the nearest neighbor interpolation (Parker et al., 1983) to eliminate the influence from different spatial resolutions. Similarly, the improvable AOD products are processed as per the correction parameters (only the data falls in the range of AOD values used to calculate the correction parameters will be corrected). For the sequence template, they are obtained for the underlying surface of nearly pure single types (>80%), while the actual land cover types are usually mixed in each grid (0.06°). It seems that the sequence template could not be directly applied. However, the spatial resolutions of the AOD products (0.06°) and the land cover types (0.005°) differ widely. Therefore, the percentage of each land cover type in the grids (0.06°) cloud be calculated, which is exactly considered as the weight (see Eq. (8)) to acquire the ideal AOD products in the mixed surface.

$$\tau_M = \sum_{l=1}^{6} p_l \tau_{SEN(s,l)} \tag{8}$$

where $\tau_{SEN(s,l)}$ represents the first valid AOD value from remote sensing sensors (MODIS and VIIRS) in the sequence template of the season s and land cover type l; $p_l$is the percentage of land cover type l; $\tau_M$denotes the merged AOD product. Compared with the commonly used empirical methods, e.g., the customized methods (Bilal et al., 2017), the proposed merging framework considers the prior information from ground truth-values and adapts an unmixing-like technique (Nascimento et al., 2005) according to land cover types. An example of merging DB_M, DT, DB_V, and EDR for one grid (i, j) is presented in Fig. 15 to clearly show the procedure. In this grid, a total of three land cover types are assumed and the season is supposed as DJF. On account of the invalid value of EDR and the valid range of DB_M, only uncorrected DB_M, DT, and DB_V (bold in the sequence template) are merged for this example.

5.2. Experiment results and discussions

To roundly evaluate the result of the proposed merging framework,

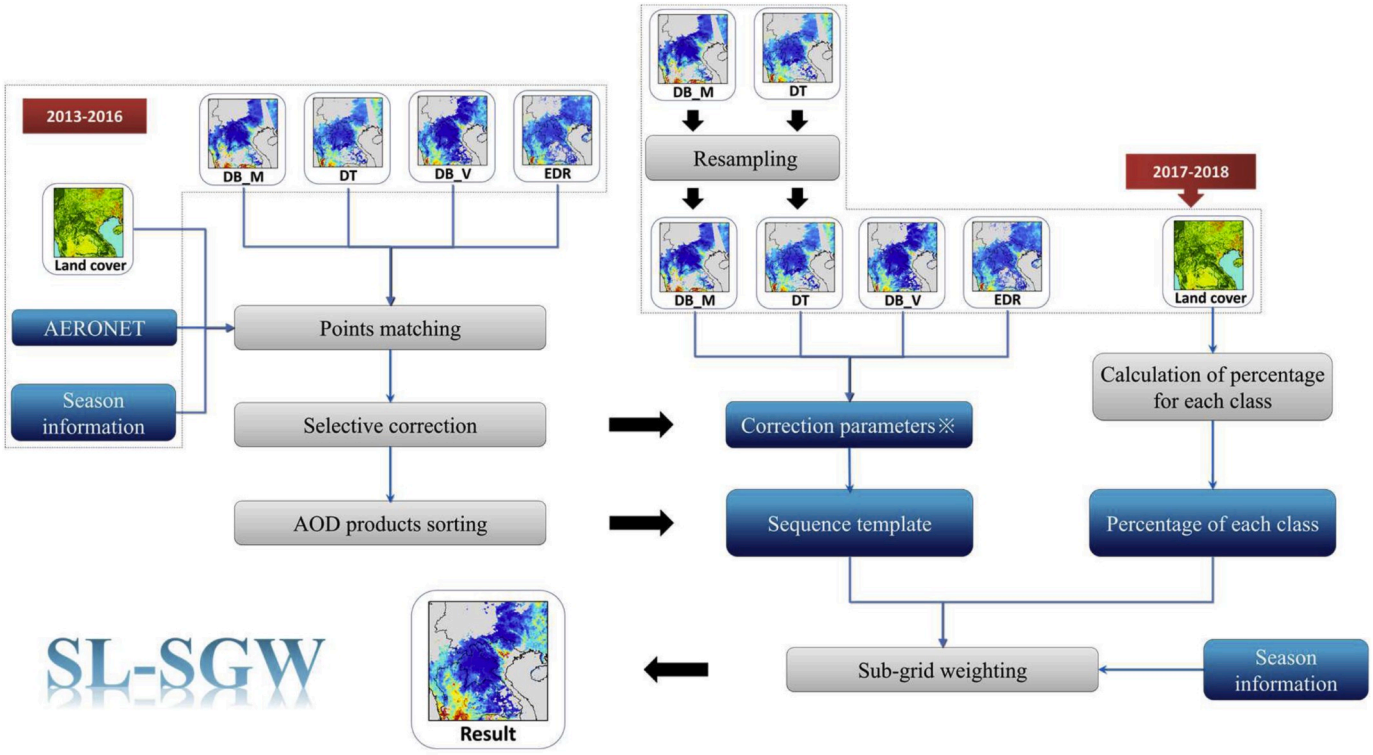

Fig. 14. The flowchart of SL-SGW. ※: only the data falls in the range of AOD values used to calculate the correction parameters will be corrected.

Coordinate	Season	P_1	P_2	P_3
i, j	DJF	34.5%	35.5%	30%

Name	DB_M	DB_M*	DT	DB_V	EDR
Value	0.18	0.25	0.22	0.19	Invalid

Season	Land cover type	Name	Valid range
DJF	1	DB_M	0.02-0.17

Season	Land cover type	Performance sequence
DJF	1	DB_M*, **DB_M**, DT, DB_V, EDR
	2	EDR, **DT**, DB_V, DB_M
	3	**DB_V**, DT, DB_M, EDR

Merged result=0.18*34.5%+0.22*35.5%+0.19*30%=0.197

Fig. 15. An example of merging DB_M, DT, DB_V, and EDR for one grid (i, j). The symbol * represents the corrected AOD product.

the land cover types are considered in the evaluation (similar to Section 3.3). As listed in Table 3, the merged AOD product achieves a good performance, seen from the counts of the top two metrics (bold and underlined). Overall, the R and the RMSE for the merged AOD product are 0.904 and 0.13, respectively. Meanwhile, the number of matched points (6086) is significantly improved compared to other AOD products (4048, 2831, 3862, and 4013). It's believed that the merging framework could effectively discard the dross and select the essence from the AOD products of DB_M, DT, DB_V, and EDR. To be specific, the underestimations of AOD values for all AOD products in *forest* are mitigated after merging, with the fraction within EE of 72.18% and the RMB of 1.04. The overestimations of AOD values for DB_M and DB_V in *arid lands* are also reduced. However, the Rs for the merged AOD product are around 0.8 in *savannas* and *grasslands*, which likely results from the bad quality of DB_M (0.755) and DT (0.425).

With regard to the completeness of valid AOD values, the annual AOD completeness during 2013–2018 of DB_M, DT, DB_V, EDR, and the merged AOD product is mapped in Fig. 16. As can be discovered, the annual AOD completeness of the merged AOD product exceeds those of DB_M, DT, DB_V, and EDR, with different degrees of improvement. For instance, the average annual AOD completeness is increased from 8.2% to 19.03%–28.69% for DT (20.49%) and DB_V (9.66%), respectively (see Table 4). By comparison to a single AOD product, the improvements of the annual AOD completeness after merging still vary in different regions of which the land cover types are diverse. As listed in Table 4, the most significant improvements are considered in the regions of *croplands* and *urban*. Even compared to the largest average annual AOD completeness in these land cover types, the increment of the average annual AOD completeness is more than 10% after merging.

Table 3
The comparison of DB_M, DT, DB_V, EDR, and the merged AOD product against AERONET during 2017–2018 for diverse land cover types. The bold and underlined denote the best and the second-best metrics, respectively. The shade of gray highlights the merged AOD product. F_A: the fraction above EE; F_W: the fraction within EE; F_B: the fraction below EE.

Land cover	Name	N	R	RMSE	Bias	F_A	F_W	F_B	RMB
All	DB_M	4048	0.871	0.17	0.023	23.59	61.71	14.7	1.07
	DT	2831	**0.909**	0.14	0.035	25.57	62.13	12.29	1.1
	DB_V	3862	0.907	**0.13**	0.013	**19.08**	**69.52**	11.39	1.04
	EDR	4013	0.798	0.17	**−0.003**	24.35	54.9	20.76	**0.99**
	Merged	**6086**	0.904	**0.13**	0.032	24.35	68.49	**7.16**	1.1
Forest	DB_M	127	0.91	0.12	−0.073	**2.36**	53.54	44.09	0.69
	DT	144	**0.927**	0.09	−0.041	8.33	59.72	31.94	0.82
	DB_V	127	0.907	0.11	−0.064	3.94	52.76	43.31	0.71
	EDR	230	0.894	0.11	−0.032	15.65	56.96	27.39	0.86
	Merged	**248**	0.926	**0.08**	**0.009**	18.15	**72.18**	**9.68**	**1.04**
Savannas	DB_M	42	0.755	0.07	−0.006	7.14	83.33	9.52	0.94
	DT	49	**0.889**	0.06	−0.014	8.16	79.59	12.24	0.89
	DB_V	39	0.888	**0.05**	−0.022	**0**	**92.31**	7.69	0.78
	EDR	49	0.875	0.06	−0.028	4.08	85.71	10.2	0.76
	Merged	**59**	0.822	0.06	**0.005**	8.47	86.44	**5.08**	**1.04**
Grasslands	DB_M	120	0.819	0.07	−0.024	**8.33**	71.67	20	0.82
	DT	100	0.425	0.14	0.105	69	30	**1**	1.75
	DB_V	177	**0.877**	**0.06**	**0**	12.99	**79.66**	7.34	**1**
	EDR	8	0.794	0.19	−0.042	12.5	37.5	50	0.86
	Merged	**219**	0.815	0.07	0.022	22.37	73.97	3.65	1.16
Croplands	DB_M	339	0.815	0.29	0.016	22.12	51.33	26.55	1.03
	DT	331	**0.919**	0.18	0.053	25.68	62.84	11.48	1.1
	DB_V	336	0.891	**0.17**	**−0.015**	13.39	**71.73**	14.88	**0.97**
	EDR	**441**	0.748	0.27	−0.129	**9.3**	44.67	46.03	0.75
	Merged	440	0.896	0.19	0.023	20.45	70.91	**8.64**	1.04
Urban	DB_M	437	0.928	0.23	0.109	38.67	57.44	3.89	1.29
	DT	155	0.927	0.26	0.212	74.84	24.52	**0.65**	1.53
	DB_V	466	**0.97**	**0.1**	**0.024**	**14.59**	**79.61**	5.79	**1.06**
	EDR	192	0.801	0.26	0.17	62.5	32.81	4.69	1.48
	Merged	**484**	0.957	0.14	0.043	17.15	79.55	3.31	1.1
Arid lands	DB_M	756	0.848	0.13	0.07	41.27	54.23	4.5	1.28
	DB_V	589	**0.895**	0.19	0.102	45.84	52.29	**1.87**	1.44
	Merged	**846**	0.87	**0.11**	**0.01**	**20.09**	**69.86**	10.05	**1.04**

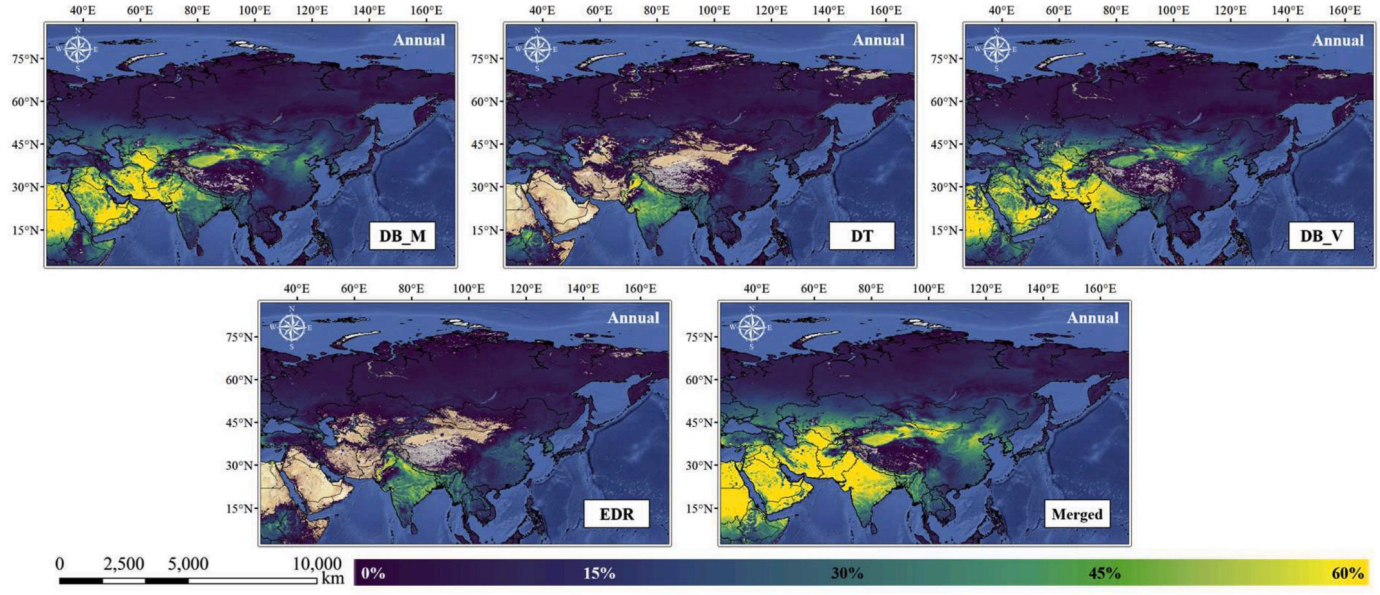

Fig. 16. The annual AOD completeness of DB_M, DT, DB_V, EDR, and the merged AOD product during 2017–2018. The base-map in this figure is the natural earth shaded map and the color bar illustrates the AOD completeness. (For interpretation of the references to color in this figure legend, the reader is referred to the Web version of this article.)

6. Conclusions

The first purpose of this paper is to evaluate and compare the latest AOD products from MODIS and VIIRS (DB_M, DT, DB_V, and EDR) during 2013–2018 in Asia. The principal conclusions are as follows: 1) Overall, the AOD product of DB_V achieves the best performance, with the R of 0.91 and the RMSE of 0.14. At the same time, the performance of DB_M and DT are acceptable, with similar metrics. On the contrary, the

Table 4
The average AOD completeness of DB_M, DT, DB_V, EDR, and the merged AOD product during 2017–2018 for diverse land cover types. The bold and underlined denote the best and the second-best metrics, respectively. The shade of gray highlights the merged AOD product.

Name	All	*Forest*	*Savannas*	*Grasslands*	*Croplands*	*Urban*	*Arid lands*
DB_M	20.99%	8.00%	8.80%	18.05%	24.59%	18.24%	47.88%
DT	8.20%	7.38%	8.28%	8.18%	23.36%	10.32%	–
DB_V	19.03%	6.39%	7.51%	17.02%	27.59%	17.68%	40.69%
EDR	8.29%	9.95%	9.95%	4.57%	22.30%	17.33%	–
Merged	**28.69%**	**13.69%**	**14.53%**	**23.83%**	**38.03%**	**28.71%**	**55.53%**

AOD quality of EDR is considered poor, of which the fraction within the EE is only 55.05%. 2) The deviations for DB_M, DT, DB_V, and EDR periodically fluctuate with different levels as time moves forward. Generally, the AOD product of DB_V overcomes others with the smallest overall deviation. Meanwhile, the largest positive and negative deviations are observed in DT and EDR, respectively. 3) The performance of each AOD product is different in the regions with diverse land cover types. Especially, all AOD products will generally underestimate the AOD values in *forest*; DB_V performs better than DB_M in *croplands* and *urban*, while the overestimation of DB_V is larger than that of DB_M in *arid lands*. 4) The distribution of high AOD values for DT and EDR shows difference in four seasons, which is dominated by multiple factors, such as anthropogenic activities. With regard to DB_M and DB_V, apart from the seasonal variations, the high AOD values also distribute in *arid lands* in MAM and JJA. Except for the bright surface, the seasonal AOD spatial distribution is similar for the AOD products of DB_M, DT, DB_V, and EDR. 5) The small annual AOD completeness of all AOD products usually distributes in the North and some islands in the South. For DB_M and DB_V, the annual AOD completeness tends to be large in the Southwest (*arid lands*). As for DT and EDR, the large annual AOD completeness principally distributes in India, where the primary land cover type is *croplands*.

Next, a novel grid-based merging framework (SL-SGW) is proposed to acquire the AOD product with the best performance and the largest AOD completeness of DB_M, DT, DB_V, and EDR as much as possible. All AOD products, AERONET measurements, land cover types, etc. during 2013–2016 are employed to establish the merging framework, while the datasets during 2017–2018 are used to evaluate the merged AOD product. The experiment results show that the R and the RMSE for the merged AOD product are 0.904 and 0.13, respectively. Meanwhile, the number of matched points (6086) is significantly improved compared to other AOD products. It's believed that the merging framework could effectively absorb the strengths of the AOD products of DB_M, DT, DB_V, and EDR. At the same time, the underestimations of the AOD values for all AOD products in *forest* and the overestimations for DB_M and DB_V in *arid lands* are both mitigated after merging. The AOD completeness of the merged exceeds those of other AOD products for all land cover types, particularly in *croplands* and *urban*.

Declaration of competing interest

The authors declare that they have no known competing financial interests or personal relationships that could have appeared to influence the work reported in this paper.

CRediT authorship contribution statement

Yuan Wang: Conceptualization, Methodology, Validation, Data curation, Software, Writing - original draft. **Qiangqiang Yuan:** Writing - review & editing, Supervision, Funding acquisition. **Huanfeng Shen:** Supervision. **Li Zheng:** Supervision. **Liangpei Zhang:** Project administration.

Acknowledgments

This work was supported by the National Natural Science Foundation of China (No. 41922008), the Strategic Priority Research Program of the Chinese Academy of Sciences (No. XDA19090104), the Fundamental Research Funds for the Central Universities of Wuhan Univeristy (No. 2042019kf0213), and the Science and Technology Major Project of Hubei Province (No. 2019AAA046). The authors would like to express our gratitude to the Atmosphere Archive and Distribution System (LAADS) for providing the AOD products of DB_M, DT, and DB_V and the land cover maps, the NOAA Comprehensive Large Array-data Stewardship System (CLASS) for providing the AOD product of EDR, and the Principle Investigators for establishing and maintaining the AERONET sites. The merged AOD product used in this study is available, which could be downloaded from this link (https://drive.google.com/open?id=18-XmNVq49GsDCDUBpqNKdFqRvD0CPWqg).

Appendix A. Supplementary data

Supplementary data to this article can be found online at https://doi.org/10.1016/j.atmosenv.2020.117548.

References

Ahn, C., Torres, O., Jethva, H., 2014. Assessment of OMI near-UV aerosol optical depth over land. J. Geophys. Res. Atmos. 119 (5), 2457–2473.
Alam, K., Trautmann, T., Blaschke, T., Subhan, F., 2014. Changes in aerosol optical properties due to dust storms in the Middle East and Southwest Asia. Remote Sens. Environ. 143, 216–227.
Al-Hamdan, M.Z., Oduor, P., Flores, A.I., Kotikot, S.M., Mugo, R., Ababu, J., Farah, H., 2014. Evaluating land cover changes in Eastern and Southern Africa from 2000 to 2010 using validated Landsat and MODIS data. Int. J. Appl. Earth Obs. 62, 8–26.
Barnes, W.L., Pagano, T.S., Salomonson, V.V., 1998. Prelaunch characteristics of the moderate resolution imaging spectroradiometer (MODIS) on EOS-AM1. IEEE Trans. Geosci. Rem. Sens. 36 (4), 1088–1100.
Bilal, M., Nichol, J.E., Nazeer, M., 2016. Evaluation of Aqua-MODIS C051 and C006 operational aerosol products using AERONET measurements over Pakistan. IEEE J. Sel. Topics Appl. Earth Observ. Remote Sens. 9, 52074–52080.
Bilal, M., Nichol, J.E., Wang, L., 2017. New customized methods for improvement of the MODIS C6 Dark Target and Deep Blue merged aerosol product. Remote Sens. Environ. 197, 115–124.
Bilal, M., Nichol, J.E., Chan, P.W., 2014. Evaluation and accuracy assessment of a Simplified Aerosol Retrieval Algorithm (SARA) over Beijing under low and high aerosol loadings and dust storms. Remote Sens. Environ. 153, 50–60.
Bilal, M., Nazeer, M., Nichol, J., Qiu, Z., Wang, L., Bleiweiss, M.P., Lolli, S., 2019. Evaluation of terra-MODIS C6 and C6. 1 aerosol products against beijing, XiangHe, and Xinglong AERONET sites in China during 2004-2014. Rem. Sens. 11 (5), 486.
Bingen, C., Robert, C.E., Stebel, K., Brühl, C., Schallock, J., Vanhellemont, F., Jumelet, J., 2017. Stratospheric aerosol data records for the climate change initiative, Development, validation and application to chemistry-climate modelling. Remote Sens. Environ. 203, 296–321.
Butt, M.J., Assiri, M.E., Ali, M.A., 2017. Assessment of AOD variability over Saudi Arabia using MODIS deep blue products. Environ. Pollut. 231, 143–153.
Canisius, F., Chen, J.M., 2007. Retrieving forest background reflectance in a boreal region from Multi-angle Imaging SpectroRadiometer (MISR) data. Remote Sens. Environ. 107 (1–2), 312–321.
Cappucci, F., Gobron, N., 2017. Benchmarking of essential climate variables, Gamma index theory and results for surface albedo and aerosol optical depth. Remote Sens. Environ. 203, 90–100.
Che, Y., Xue, Y., Guang, J., She, L., Guo, J., 2018. Evaluation of the AVHRR DeepBlue aerosol optical depth dataset over mainland China. ISPRS J. Photogrammetry Remote Sens. 146, 74–90.
Della Ceca, L.S., Ferreyra, M.F.G., Lyapustin, A., Chudnovsky, A., Otero, L., Carreras, H., Barnaba, F., 2018. Satellite-based view of the aerosol spatial and temporal

variability in the Córdoba region (Argentina) using over ten years of high-resolution data. ISPRS J. Photogrammetry Remote Sens. 145, 250–267.
Eck, T.F., Holben, B.N., Dubovik, O., Smirnov, A., Goloub, P., Chen, H.B., Ji, Q., 2005. Columnar aerosol optical properties at AERONET sites in central eastern Asia and aerosol transport to the tropical mid-Pacific. J. Geophys. Res. Atmos. 110 (D6).
Fan, J., Wang, Y., Rosenfeld, D., Liu, X., 2016. Review of aerosol–cloud interactions: mechanisms, significance, and challenges. J. Atmos. Sci. 73 (11), 4221–4252.
Giles, D.M., Sinyuk, A., Sorokin, M.G., Schafer, J.S., Smirnov, A., Slutsker, I., Welton, E. J., 2019. Advancements in the Aerosol Robotic Network (AERONET) Version 3 database–automated near-real-time quality control algorithm with improved cloud screening for Sun photometer aerosol optical depth (AOD) measurements. Atmos. Meas. Tech. 12 (1), 169–209.
Giles, D.M., Holben, B.N., Eck, T.F., Sinyuk, A., Smirnov, A., Slutsker, I., Schafer, J.S., 2012. An analysis of AERONET aerosol absorption properties and classifications representative of aerosol source regions. J. Geophys. Res. Atmos. 117 (D17).
Guo, J., Lou, M., Miao, Y., Wang, Y., Zeng, Z., Liu, H., Zhai, P., 2017b. Trans-Pacific transport of dust aerosols from East Asia, Insights gained from multiple observations and modeling. Environ. Pollut. 230, 1030–1039.
Guo, J., Xia, F., Zhang, Y., Liu, H., Li, J., Lou, M., Zhai, P., 2017a. Impact of diurnal variability and meteorological factors on the PM2. 5-AOD relationship, Implications for PM2. 5 remote sensing. Environ. Pollut. 221, 94–104.
Guo, J., Deng, M., Lee, S.S., Wang, F., Li, Z., Zhai, P., Li, X., 2016. Delaying precipitation and lightning by air pollution over the Pearl River Delta. Part I: observational analyses. J. Geophys. Res. Atmos. 121 (11), 6472–6488.
Guo, J., Liu, H., Li, Z., Rosenfeld, D., Jiang, M., Xu, W., Zhai, P., 2018. Aerosol-induced changes in the vertical structure of precipitation: a perspective of TRMM precipitation radar. Atmos. Chem. Phys. 18 (18).
Gupta, P., Levy, R.C., Mattoo, S., Remer, L.A., Munchak, L.A., 2016. A surface reflectance scheme for retrieving aerosol optical depth over urban surfaces in MODIS Dark Target retrieval algorithm. Atmos. Meas. Tech. 9 (7), 3293–3308.
He, Q., Li, C., Tang, X., Li, H., Geng, F., Wu, Y., 2010. Evaluation of MODIS derived aerosol optical depth over the Yangtze River Delta in China. Remote Sens. Environ. 114, 81649–81661.
He, Q., Zhang, M., Huang, B., 2016. Spatio-temporal variation and impact factors analysis of satellite-based aerosol optical depth over China from 2002 to 2015. Atmos. Environ. 129, 79–90.
He, Q., Zhang, M., Huang, B., Tong, X., 2017. Modis 3km and 10km aerosol optical depth for China, evaluation and comparison. Atmos. Environ. 153, 150–162.
Holben, B.N., Tanre, D., Smirnov, A., Eck, T.F., Slutsker, I., Abuhassan, N., Kaufman, Y.J., 2001. An emerging ground-based aerosol climatology, Aerosol optical depth from AERONET. J. Geophys. Res. Atmos. 106, D1112067–D1112097.
Holben, B.N., Eck, T.F., Slutsker, I., Tanre, D., Buis, J.P., Setzer, A., Lavenu, F., 1998. AERONET—a federated instrument network and data archive for aerosol characterization. Remote Sens. Environ. 66 (1), 1–16.
Hsu, N.C., Tsay, S.C., King, M.D., Herman, J.R., 2004. Aerosol properties over bright-reflecting source regions. IEEE Trans. Geosci. Rem. Sens. 42 (3), 557–569.
Hsu, N.C., Jeong, M.J., Bettenhausen, C., Sayer, A.M., Hansell, R., Seftor, C.S., Tsay, S.C., 2013. Enhanced Deep Blue aerosol retrieval algorithm, the second generation. J. Geophys. Res. Atmos. 118 (16), 9296–9315.
Hsu, N.C., Lee, J., Sayer, A.M., Kim, W., Bettenhausen, C., Tsay, S.C., 2019. VIIRS deep blue aerosol products over land, extending the EOS long-term aerosol data records. J. Geophys. Res. Atmos. 124 (7), 4026–4053.
Huang, R.J., Zhang, Y., Bozzetti, C., Ho, K.F., Cao, J.J., Han, Y., Zotter, P., 2014. High secondary aerosol contribution to particulate pollution during haze events in China. Nature 514 (7521), 218.
Jackson, J.M., Liu, H., Laszlo, I., Kondragunta, S., Remer, L.A., Huang, J., Huang, H.C., 2013. Suomi-NPP VIIRS aerosol algorithms and data products. J. Geophys. Res. Atmos. 118 (22), 12–673.
Kahn, R.A., Gaitley, B.J., Garay, M.J., Diner, D.J., Eck, T.F., Smirnov, A., Holben, B.N., 2010. Multiangle imaging SpectroRadiometer global aerosol product assessment by comparison with the aerosol robotic network. J. Geophys. Res. Atmos. 115 (D23).
Kaskaoutis, D.G., Badarinath, K.V.S., Kumar Kharol, S., Rani Sharma, A., Kambezidis, H. D., 2009. Variations in the aerosol optical properties and types over the tropical urban site of Hyderabad, India. J. Geophys. Res. Atmos. 114 (D22).
Kaufman, Y.J., Tanré, D., Boucher, O., 2002. A satellite view of aerosols in the climate system. Nature 419, 6903215–6903223.
Kaufman, Y.J., Koren, I., Remer, L.A., Tanré, D., Ginoux, P., Fan, S., 2005. Dust transport and deposition observed from the terra-moderate resolution imaging spectroradiometer (MODIS) spacecraft over the Atlantic ocean. J. Geophys. Res. Atmos. 110, D10.
Kharol, S.K., Badarinath, K.V.S., Sharma, A.R., Kaskaoutis, D.G., Kambezidis, H.D., 2011. Multiyear analysis of Terra/Aqua MODIS aerosol optical depth and ground observations over tropical urban region of Hyderabad, India. Atmos. Environ. 45 (8), 1532–1542.
Levy, R.C., Mattoo, S., Munchak, L.A., Remer, L.A., Sayer, A.M., Patadia, F., Hsu, N.C., 2013. The Collection 6 MODIS aerosol products over land and ocean. Atmos. Meas. Tech. 6 (11).
Levy, R.C., Remer, L.A., Mattoo, S., Vermote, E.F., Kaufman, Y.J., 2007. Second-generation operational algorithm, Retrieval of aerosol properties over land from inversion of Moderate Resolution Imaging Spectroradiometer spectral reflectance. J. Geophys. Res. Atmos. 112, D13.
Li, S., Chen, L., Tao, J., Han, D., Wang, Z., Su, L., Yu, C., 2012. Retrieval of aerosol optical depth over bright targets in the urban areas of North China during winter. Sci. China Earth Sci. 55 (9), 1545–1553.
Li, L., Yang, J., Wang, Y., 2014. An improved dark object method to retrieve 500 m-resolution AOT (Aerosol Optical Thickness) image from MODIS data: a case study in the Pearl River Delta area, China. ISPRS J. Photogrammetry Remote Sens. 89, 1–12.
Li, T., Shen, H., Yuan, Q., Zhang, X., Zhang, L., 2017a. Estimating ground-level PM2. 5 by fusing satellite and station observations: a geo-intelligent deep learning approach. Geophys. Res. Lett. 44 (23), 11–985.
Li, Z., Guo, J., Ding, A., Liao, H., Liu, J., Sun, Y., Zhu, B., 2017b. Aerosol and boundary-layer interactions and impact on air quality. Natl. Sci. Rev. 4 (6), 810–833.
Li, Z., Wang, Y., Guo, J., Zhao, C., Cribb, M.C., Dong, X., Jiang, Y., 2019. East Asian study of tropospheric aerosols and their impact on regional clouds, precipitation, and climate (EAST-AIRCPC). J. Geophys. Res. Atmos. 124 (23), 13026–13054.
Liu, H., Remer, L.A., Huang, J., Huang, H.C., Kondragunta, S., Laszlo, I., Jackson, J.M., 2014. Preliminary evaluation of S-NPP VIIRS aerosol optical thickness. J. Geophys. Res. Atmos. 119 (7), 3942–3962.
Liu, N., Zou, B., Feng, H., Wang, W., Tang, Y., Liang, Y., 2019. Evaluation and comparison of multiangle implementation of the atmospheric correction algorithm, Dark Target, and Deep Blue aerosol products over China. Atmos. Chem. Phys. 19 (12), 8243–8268.
Lohmann, U., Feichter, J., 2001. Can the direct and semi-direct aerosol effect compete with the indirect effect on a global scale? Geophys. Res. Lett. 28 (1), 159–161.
Mhawish, A., Banerjee, T., Broday, D.M., Misra, A., Tripathi, S.N., 2017. Evaluation of MODIS Collection 6 aerosol retrieval algorithms over Indo-Gangetic Plain, Implications of aerosols types and mass loading. Remote Sens. Environ. 201, 297–313.
Mhawish, A., Banerjee, T., Sorek-Hamer, M., Lyapustin, A., Broday, D.M., Chatfield, R., 2019. Comparison and evaluation of MODIS multi-angle implementation of atmospheric correction (MAIAC) aerosol product over South Asia. Remote Sens. Environ. 224, 12–28.
Nascimento, J.M., Dias, J.M., 2005. Vertex component analysis: a fast algorithm to unmix hyperspectral data. IEEE Trans. Geosci. Rem. Sens. 43 (4), 898–910.
Parker, J.A., Kenyon, R.V., Troxel, D.E., 1983. Comparison of interpolating methods for image resampling. IEEE Trans. Med. Imag. 2 (1), 31–39.
Ramanathan, V.C.P.J., Crutzen, P.J., Kiehl, J.T., Rosenfeld, D., 2011. Aerosols, climate, and the hydrological cycle. Science 294 (5549), 2119–2124.
Rosenfeld, D., Sherwood, S., Wood, R., Donner, L., 2014. Climate effects of aerosol-cloud interactions. Science 343 (6169), 379–380.
Sayer, A.M., Hsu, N.C., Bettenhausen, C., Ahmad, Z., Holben, B.N., Smirnov, A., Zhang, J., 2012. SeaWiFS Ocean Aerosol Retrieval (SOAR), Algorithm, validation, and comparison with other data sets. J. Geophys. Res. Atmos. 117 (D3).
Sayer, A.M., Hsu, N.C., Bettenhausen, C., Jeong, M.J., Meister, G., 2015. Effect of MODIS Terra radiometric calibration improvements on collection 6 deep blue aerosol products, validation and terra/aqua consistency. J. Geophys. Res. Atmos. 120 (23), 12–157.
Sayer, A.M., Munchak, L.A., Hsu, N.C., Levy, R.C., Bettenhausen, C., Jeong, M.J., 2014. MODIS Collection 6 aerosol products, Comparison between Aqua's e-Deep Blue, Dark Target, and "merged" data sets, and usage recommendations. J. Geophys. Res. Atmos. 119 (24), 13–965.
Sayer, A.M., Hsu, N.C., Lee, J., Kim, W.V., Dutcher, S.T., 2019. Validation, stability, and consistency of MODIS Collection 6.1 and VIIRS Version 1 Deep Blue aerosol data over land. J. Geophys. Res. Atmos. 124 (8), 4658–4688.
Shen, H., Li, T., Yuan, Q., Zhang, L., 2018. Estimating regional ground-level PM2. 5 directly from satellite top-of-atmosphere reflectance using deep belief networks. J. Geophys. Res. Atmos. 123 (24), 13–875.
Tang, Q., Bo, Y., Zhu, Y., 2016. Spatiotemporal fusion of multiple-satellite aerosol optical depth (AOD) products using Bayesian maximum entropy method. J. Geophys. Res. Atmos. 121 (8), 4034–4048.
Tian, X., Liu, Q., Li, X., Wei, J., 2018. Validation and comparison of MODIS C6. 1 and C6 aerosol products over beijing, China. Rem. Sens. 10 (12), 2021.
Twomey, S., 1977. The influence of pollution on the shortwave albedo of clouds. J. Atmos. Sci. 34 (7), 1149–1152.
Virtanen, T.H., Kolmonen, P., Sogacheva, L., Rodríguez, E., Saponaro, G., de Leeuw, G., 2018. Collocation mismatch uncertainties in satellite aerosol retrieval validation. Atmos. Meas. Tech. 11 (2), 925.
Wang, Y., Yuan, Q., Li, T., Shen, H., Zheng, L., Zhang, L., 2019a. Evaluation and comparison of MODIS Collection 6.1 aerosol optical depth against AERONET over regions in China with multifarious underlying surfaces. Atmos. Environ. 200, 280–301.
Wang, Y., Yuan, Q., Li, T., Shen, H., Zheng, L., Zhang, L., 2019b. Large-scale MODIS AOD products recovery, Spatial-temporal hybrid fusion considering aerosol variation mitigation. ISPRS J. Photogrammetry Remote Sens. 157, 1–12.
Wang, Z., Schaaf, C.B., Strahler, A.H., Chopping, M.J., Román, M.O., Shuai, Y., Fitzjarrald, D.R., 2014. Evaluation of MODIS albedo product (MCD43A) over grassland, agriculture and forest surface types during dormant and snow-covered periods. Remote Sens. Environ. 140, 60–77.
Wang, L., Gong, W., Xia, X., Zhu, J., Li, J., Zhu, Z., 2015. Long-term observations of aerosol optical properties at Wuhan, an urban site in Central China. Atmos. Environ. 101, 94–102.
Wei, J., Sun, L., Huang, B., Bilal, M., Zhang, Z., Wang, L., 2017. Verification, improvement and application of aerosol optical depths in China Part 1, Inter-comparison of NPP-VIIRS and Aqua-MODIS. Atmos. Environ. 175, 221–233.
Wei, J., Peng, Y., Mahmood, R., Sun, L., Guo, J., 2019. Intercomparison in spatial distributions and temporal trends derived from multi-source satellite aerosol products. Atmos. Chem. Phys. 19 (10), 7183–7207.
Xiong, X., Butler, J., Chiang, K., Efremova, B., Fulbright, J., Lei, N., Wu, A., 2014. VIIRS on-orbit calibration methodology and performance. J. Geophys. Res. Atmos. 119 (9), 5065–5078.

Yang, Q., Yuan, Q., Yue, L., Li, T., Shen, H., Zhang, L., 2019. The relationships between PM2. 5 and aerosol optical depth (AOD) in mainland China: about and behind the spatio-temporal variations. Environ. Pollut. 248, 526–535.
Yang, X., Zhao, C., Zhou, L., Wang, Y., Liu, X., 2016. Distinct impact of different types of aerosols on surface solar radiation in China. J. Geophys. Res. Atmos. 121 (11), 6459–6471.
Zhang, Z., Wu, W., Fan, M., Tao, M., Wei, J., Jin, J., Wang, Q., 2019. Validation of Himawari-8 aerosol optical depth retrievals over China. Atmos. Environ. 199, 32–44.
Zou, B., You, J., Lin, Y., Duan, X., Zhao, X., Fang, X., Li, S., 2019. Air pollution intervention and life-saving effect in China. Environ. Int. 125, 529–541.